FINNISH METEOROLOGICAL INSTITUTE
CONTRIBUTIONS

No. 102

# ATMOSPHERIC ICE AND DUST: FROM MORPHOLOGICAL MODELING TO LIGHT SCATTERING

Hannakaisa Lindqvist

Department of Physics
Faculty of Science
University of Helsinki
Helsinki, Finland

ACADEMIC DISSERTATION in meteorology

To be presented, with the permission of the Faculty of Science of the University of Helsinki, for public criticism in Physicum auditorium E204, Gustaf Hällströmin katu 2, on December 19th, 2013, at 12 o'clock noon.

Finnish Meteorological Institute
Helsinki, 2013

ISBN 978-951-697-811-9 (paperback)
ISSN 0782-6117
Unigrafia
Helsinki, 2013

ISBN 978-951-697-812-6 (PDF)
Helsinki, 2013

FINNISH METEOROLOGICAL INSTITUTE

Published by Finnish Meteorological Institute

P.O. Box 503
FIN-00101 Helsinki, Finland

Series title, number and report code of publication
Finnish Meteorological Institute
Contributions 102, FMI-CONT-102

Date
November 2013

Author
Hannakaisa Lindqvist

Title
Atmospheric ice and dust: From morphological modeling to light scattering

Abstract

The atmosphere of the Earth contains a rich variety of small particles that contribute to numerous local and global meteorological phenomena, such as visibility, water circulation, and climate change. Of particular relevance for this thesis, the particles scatter and absorb solar light and, therefore, are significant to the radiative balance of the Earth-atmosphere system. Likewise, they influence remote-sensing observations and can be monitored through the radiation they scatter.

The interaction between radiation and the individual particles cannot be accurately established without modeling the physics of scattering and absorption. In the case of spherical particles, such as water droplets in low-altitude clouds, this is straightforward because an analytical solution exists, but solid-form particles are not spherical. They need models for their morphology, and dedicated computational methods to solve their scattering properties. Radiatively most important classes of nonspherical atmospheric particles are ice crystals in high-altitude clouds and dust aerosol particles, including both volcanic and mineral dust. Both scattering and absorption are generally known to be sensitive to the physical properties of the particles – size, shape, and composition – and yet, these ice and dust particles are currently modeled with overly simplistic and not properly validated approaches in many key applications, including climate models.

In the thesis, light scattering by atmospheric ice and dust particles is investigated using morphologically faithful models that take into account the shape, internal structure, and material inhomogeneity. Detailed models are developed for small ice crystals, whose shapes have been controversial due to lack of knowledge, and for volcanic dust particles, whose porosity greatly impacts their scattering properties: an effect that is usually ignored. As a major highlight, the thesis presents a paradigm change in modeling scattering by mineral dust by introducing a first-ever model that has been derived directly from the observed shape and inhomogeneous composition of individual, micrometer-scale mineral dust particles. For ice crystals, the thesis introduces a fully automatic shape classification algorithm, which greatly facilitates the analysis of ice cloud microphysical data and, hence, the computation of cloud radiative effect. Selected results of the thesis are already in use in multidisciplinary applications; in atmospheric sciences, the results have led to more accurate radiative impact estimations and simulations of the entire climate.

Publishing unit
Finnish Meteorological Institute

Classification (UDC)
551.521.3
551.574.13

Keywords
light scattering and absorption
ice particles in clouds
dust aerosols

ISSN and series title
0782-6117 Finnish Meteorological Institute Contributions

ISBN
978-951-697-811-9 (paperback), 978-951-697-812-6 (PDF)

Language
English

Pages
154

Price

Sold by
Finnish Meteorological Institute
P.O. Box 503, FIN-00101 Helsinki, Finland

Note

ILMATIETEEN LAITOS

Julkaisija
Ilmatieteen laitos

PL 503
00101 Helsinki

Julkaisun sarja, numero ja raporttikoodi
Finnish Meteorological Institute
Contributions 102, FMI-CONT-102

Julkaisuaika
Marraskuu 2013

Tekijä
Hannakaisa Lindqvist

Nimike
Ilmakehän jää- ja pölyhiukkaset: muotomallituksesta valonsirontaan

Tiivistelmä

Pienhiukkaset vaikuttavat monella tärkeällä tavalla ilmakehän eri prosesseihin ja ilmiöihin. Esimerkiksi pilvien muodostumisen ja veden kiertokulun osalta niiden merkitys on hyvin keskeinen. Tässä väitöskirjassa tarkastellaan erityisesti pienhiukkasten vuorovaikutusta Auringon säteilyn kanssa. Säteilyn sironta ja absorptio liittyvät läheisesti ilmakehän säteilytasapainoon ja ilmaston mallintamiseen, ja lisäksi hiukkasia voidaan havaita ja tutkia niiden sirottaman säteilyn kautta.

Auringon säteilyn ja yksittäisen hiukkasen vuorovaikutusta käsitellään sähkömagneettisena sirontana. Pallomaisten hiukkasten, kuten pilvipisaroiden, sirontaa kuvaavat yhtälöt ratkeavat analyyttisesti. Ilmakehässä on kuitenkin myös erityyppisiä kiinteän olomuodon hiukkasia: esimerkiksi yläpilvien jääkiteitä ja maaperästä lähtöisin olevaa mineraalipölyä. Näiden hiukkasten muoto ja mineraalipölyn tapauksessa myös koostumus vaihtelevat. Hiukkasen koko, muoto ja koostumus vaikuttavat valonsirontaan tutkitusti paljon; siitä huolimatta näitä hiukkasia mallinnetaan edelleen suhteellisen yksinkertaisin mallein keskeisissä sovelluksissa, esimerkiksi ilmastomalleissa.

Väitöskirjassa keskitytään ilmakehän jääkiteiden sekä mineraali- ja tulivuoripölyhiukkasten valonsironnan mallinnukseen. Hiukkasten muoto, koostumus ja sisäinen rakenne huomioidaan, ja työssä selvitetään näiden ominaisuuksien vaikutusta valonsirontaan. Yksityiskohtaiset mallinnustavat esitetään rakenteeltaan huokoiselle tulivuoripölylle sekä pienille jääkiteille, joita ei kyetä nykyisin keinoin havaitsemaan tarpeeksi tarkasti. Väitöskirjassa luodaan myös täysin automaattinen jääkiteiden muotoluokitin, jonka avulla voidaan tehokkaasti analysoida mittaustuloksia yläpilvien mikrofysiikasta ja hyödyntää tuloksia esimerkiksi pilvien heijastavuuden ja absorption arvioinnissa. Mineraalipölyn mallinnukseen esitellään tieteenalalla käänteentekevä askel: väitöskirjassa selvitetään mineraalipölyhiukkasen kolmiulotteinen muoto ja mineraalikoostumus suoraan havainnoista stereogrammetrian ja spektroskopian avulla, ja näin saatua pölyhiukkasen mallia hyödynnetään sellaisenaan sirontamallituksessa. Osaa väitöskirjan tuloksista on jo sovellettu aiempaa tarkempiin säteilynkulkutarkasteluihin ja edelleen ilmastosimulaatioihin. Ilmakehätieteiden lisäksi myös muilla tieteenaloilla voidaan soveltaa työssä esiteltyjä menetelmiä ja tuloksia.

Julkaisijayksikkö
Ilmatieteen laitos

Luokitus (UDK)
551.521.3
551.574.13

Asiasanat
valonsironta ja absorptio ilmakehässä
jääpilvipartikkelit
pölyaerosolit

ISSN ja avainnimike
0782-6117 Finnish Meteorological Institute Contributions

ISBN
978-951-697-811-9 (paperback), 978-951-697-812-6 (PDF)

Kieli
englanti

Sivumäärä
154

Hinta

Myynti
Ilmatieteen laitos
PL 503, 00101 Helsinki

Lisätietoja

# Preface

The research for this thesis was carried out during the years 2008-2013 at the Department of Physics, University of Helsinki. As an astronomy graduate specialized in planetary science, my knowledge of the atmosphere of this particular planet was on quite general level, to begin with. Therefore, I want to first thank my advisor, Dr. Timo Nousiainen, for having enough faith in me to offer me the opportunity to work for a PhD in meteorology. With Timo's guidance, I have found a profound motivation to study the atmosphere and also continue research on this field. My second advisor, prof. Karri Muinonen, was the one who convinced me to continue to the PhD after my master's degree. Discussions with him tend to be highly inspirational and leave me under the positive, but usually false, impression that all my research problems have been solved. I thank both my advisors for sharing their neverending enthusiasm towards research, but also for giving me teaching and other responsibilities that made my work very versatile.

One of the most important things Timo has taught me is the value of collaboration. I have indeed learned a lot from my co-authors: Timo, Karri, Olga, Evgenij, Sini, Michael, Greg, Jun, Päivi, Risto, Hanne, Olli, Konrad, and Dirk are acknowledged for their contributions to the publications of this thesis. In particular, I wish to thank Päivi for not just sharing an office with me but for sharing the everyday excitement as well. Also, I thank all the unique people in Atmospheric radiation group and Planetary system research group for advice, ideas, and good conversations.

I would also like to acknowledge the colleagues in the international light-scattering community. Especially, Dr. Anthony Baran and Dr. Matthew Berg pre-examined this thesis and gave constructive remarks for improving it. Furthermore, Dr. Maxim Yurkin, Dr. Bruce Draine, and Dr. Michael Mishchenko are acknowledged for making their light-scattering codes publicly available. Computations were made feasible by the resources granted by CSC - IT Center for Science Ltd. and the Department of Physics. Research conducted for this thesis would not have been possible without funding from the Academy of Finland (project 125180) and prof. Markku Kulmala.

Throughout my studies, I have been lucky to have the support of my friends and family. I want to thank my friends for all distraction in the form of board games, dinner parties, and sauna evenings. Also, the mutual support from those also finalizing their theses has been invaluable. As for the family, my parents Heli and Pekka could not have done more to encourage me and my siblings to be interested in nature and its phenomena. I wonder if they knew where this would lead me, and I can't wait to give similar experiences to my daughter Ilona. Finally, I wish to thank my husband Tuomo most dearly for never failing to support me in anything I decide to do.

Helsinki, November 2013

Hannakaisa Lindqvist

# Contents

# Original publications

This thesis consists of an introductory review, followed by six peer-reviewed research articles. In the introductory part, these papers are cited according to their roman numerals.

I Lindqvist, H., Muinonen, K., and Nousiainen, T. (2009). Light scattering by coated Gaussian and aggregate particles, *J. Quant. Spectrosc. Radiat. Transfer*, 110:1398–1410.

II Lindqvist, H., Nousiainen, T., Zubko, E., and Muñoz, O. (2011). Optical modeling of vesicular volcanic ash particles, *J. Quant. Spectrosc. Radiat. Transfer*, 112:1871–1880.

III Merikallio, S., Lindqvist, H., Nousiainen, T., and Kahnert, M. (2011). Modelling light scattering by mineral dust using spheroids: assessment of applicability, *Atmos. Chem. Phys.*, 11:5347–5363.

IV Nousiainen, T., Lindqvist, H., McFarquhar, G. M., and Um, J. (2011). Small irregular ice crystals in tropical cirrus, *J. Atmos. Sci.*, 68:2614–2627.

V Lindqvist, H., Muinonen, K., Nousiainen, T., Um, J., McFarquhar, G. M., Haapanala, P., Makkonen, R., and Hakkarainen, H. (2012). Ice-cloud particle habit classification using principal components, *J. Geophys. Res.*, 117, D16206.

VI Lindqvist, H., Jokinen, O., Kandler, K., Scheuvens, D., and Nousiainen, T. (2013). Single scattering by realistic, inhomogeneous mineral dust particles with stereogrammetric shapes, *Atmos. Chem. Phys.*, in press.

# 1 Introduction

The atmosphere of the Earth is an endless reservoir of various particles, most of them small enough to be invisible to the human eye but observable through the radiation they collectively scatter. Rainbows, halos, glories, and coronas are beautiful indications of the presence of raindrops, ice crystals, cloud droplets, and various dust and pollen particles in our atmosphere, not to mention the colours of the sky itself: the bright blue of the daylight and the red hues of a sunset resulting from Rayleigh scattering by atmospheric gas molecules themselves [Rayleigh, 1899]. Even though the optical phenomena are fairly common, the particles and their light scattering still remain as a source of intriguing scientific questions of utmost importance, related to their characterization through remote sensing and their unresolved role in the climate change.

Aerosols and cloud particles affect numerous meteorological processes of different scales, varying from micrometeorology and local weather to global radiative balance and climate change. Mineral dust aerosol particles are crucial as a major source of nutrients for organisms in the oceans while cloud particles participate in the global water circulation. Aerosol particles are also recognized as a potential source of respiratory health issues and, especially, volcanic dust aerosol particles pose a threat to air traffic. Dust and ice particles are also linked, because dust aerosols frequently act as cloud condensation and freezing nuclei while ice crystals participate in dust particle removal from the atmosphere. For investigating all these aspects, atmospheric particles are constantly monitored through many remote-sensing systems that measure the scattered radiation either actively by first emitting the radiation and then measuring its scattering (typically backscatter), or passively by measuring scattered solar radiation or emitted thermal radiation.

The ongoing climate change is, most profoundly, a consequence of the imbalance between the incoming and outgoing radiative energy in the Earth-atmosphere system. The current imbalance is mostly caused by the increase of anthropogenic greenhouse gas emissions, mainly carbon dioxide and methane, and is rebalanced by an increase in the tropospheric and surface temperature, which increase the longwave thermal radiation [IPCC, 2007]. Although atmospheric particles affect, through scattering and absorption, the radiative balance of the atmosphere, their contribution to the direct forcing that drives the climate change is estimated to be small. Although only about 25% of atmospheric mineral dust is estimated to be of anthropogenic origin [e.g., a consequence of land use, Ginoux et al., 2012], its contribution is nevertheless notable: as important cloud condensation and freezing nuclei, the aerosol particles are related to changes in total cloud coverage and droplet/crystal size, i.e. changes in the cloud reflectivity, which is referred to as the indirect radiative forcing of aerosols. Still, estimating radiative forcing effects is not the full story when considering the relevance of atmospheric particles to climate change: it is equally important to predict what the role of the particles is in the changed climate, i.e. their response and climate sensitivity. For instance, in the case of ice cloud particles, this is yet poorly known [IPCC, 2007].

The challenges of scattering lie in the complex interaction between the particle and the incident radiation. Electromagnetic radiation, be it visible light or radiation at other wavelengths, is characterized by its wavelength and polarization state. The interaction means that the electric field of the incident radiation forces the charged elementary particles in an oscillatory motion, which then makes the particle reradiate, i.e., scatter, the given electromagnetic energy in all directions. In classical elastic scattering, the wavelength of the scattered light is identical to that of the incident light; however, the polarization state changes in the interaction — this is explained in more detail in Chapter 3. In the interaction, it is essential how the charges are distributed; macroscopically, this means that the shape, size, internal structure, and composition — hereafter referred to as physical properties — of the particle are significant factors. Moreover, the geometry of the settings needs to be defined so that the properties of the scattered radiation can be quantified and compared. Let us now visualize an example of the geometric aspects of the settings in the case of atmospheric ice crystals: the observer is looking at a winter sky covered with hazy cirrostratus clouds in daylight. Sunlight is incident on plate-like hexagonal ice crystals which then scatter light in all directions; however, certain directions are more prominent than others. The scattering plane is determined by the Sun, the ice crystal, and the observer, and the angle measured from the propagation direction of incident light to the direction of scattered light defines the scattering angle $\theta$, as presented in Fig. 1.1. The observer sees a halo phenomenon at an angular distance of $\theta \approx 22^\circ$ from the Sun. The halo can be either a circular 22° halo or parhelia, i.e. sundogs, depending on whether the crystals in the cloud are oriented randomly in all directions or only horizontally.

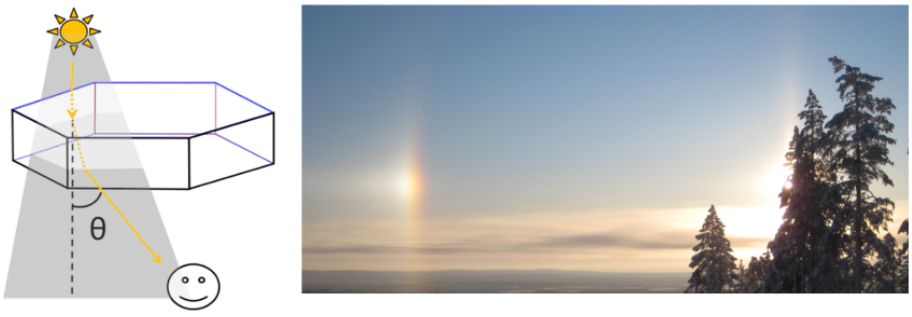


Figure 1.1: Left: definitions of the scattering angle $\theta$ and the scattering plane (shaded area). Right: parhelion — an indication of horizontally oriented hexagonal ice crystals.

The interrelation of the properties of scattered radiation and the physical properties of the particle is anything but straightforward, and there are essentially two ways of approaching the topic. If the physical properties of the particle are known, the scattered radiation can be computed using a suitable computational method (selected methods are presented in Chapter 3); this is called the direct problem. Even though the direct problem is, in itself, challenging enough, the opposite, which is called the inverse problem, is even more challenging: in the inverse problem, the physical properties of the particle are derived from the scattered radiation. With halos and ice crystals, an example of a direct problem would be to solve all possible halo shapes for a given crystal, whereas the inverse would mean that one should conclude the shape of the crystal that is causing the observed halo. In fact, even though halos have been intensively studied, unresolved mysteries

remain regarding the explanation of certain rarely seen halos whereas ready explanations exist for halos that have not yet been observed [Riikonen, 2011; Tape and Moilanen, 2006]. Finnish halo enthusiasts have been particularly active, innovative, and successful in their attempts to solve these enigmas [e.g., Riikonen et al., 2007].

In practice, solving the inverse problem requires also the solution of the direct problem; this is exactly the case when characterizing atmospheric aerosol particles through remote sensing, or identifying their contribution to other remote-sensing data, such as greenhouse gas monitoring with the GOSAT (Greenhouse Gases Observing Satellite) or OCO-2 (Orbiting Carbon Observatory -2) satellites. Radiation observed by an instrument is interpreted with the help of retrieval algorithms or lookup tables that have been constructed by solving the direct problem using light scattering simulations. For example, the ground-based AERONET (Aerosol Robotic Network) photometers measure the solar and sky radiances to infer the radiation scattered by aerosol particles, and satellite-based aerosol retrievals are made with, e.g., CALIPSO (Cloud-Aerosol Lidar and Infrared Pathfinder Satellite Observations) satellite and MODIS (Moderate-resolution Imaging Spectroradiometer) instrument onboard the Terra and Aqua satellites. The CloudSat satellite monitors clouds with radar, and is orbiting in the A-train satellite constellation together with the CALIPSO, Aqua, and Aura satellites. The inversion algorithms used in the AERONET and satellite data to retrieve the properties of aerosols are currently largely based on a database of scattering by spheroids, a simple class of nonspherical particles [Dubovik et al., 2006]. While an obvious improvement over spherical model particles, the model should be considered a stepping stone towards more realistic treatments.

Let me now briefly describe the particles considered in the thesis. The publications included in the thesis are focused on atmospheric ice and dust; including both mineral and volcanic dust. A common feature of these particles is that they have nonspherical — even irregular — shapes, with possibly inhomogeneous internal structure, and their size typically varies from submicron to hundreds of micrometers or, for ice crystals, greater than a millimeter in diameter. While their physical properties are briefly summarized in Chapter 2, it is instructive to emphasize the natural variability of morphology within these three particle categories using images of each, see Fig. 1.2.

The challenge in modeling scattering by atmospheric ice and dust is not only the obvious difficulties in the development of models that are sufficiently realistic as well as representative of their natural counterparts, but more importantly, the accurate solution of the electromagnetic interaction between incident radiation and the particle. An exact, analytical solution is possible only in a limited number of special cases, for example a homogeneous sphere, an infinite circular cylinder, and a coated sphere, for which the solutions and Fortran codes are available, e.g., in Bohren and Huffman [1983]. Otherwise, approximations generally cannot be avoided. The question is whether to approximate the properties of the particle or the physics of scattering; often, both approximations are, to some extent, necessary. The lack of an analytical solution in the general case unfortunately means longer computational times, sometimes unbearably so, depending on the numerical methods employed, and typically result in a limited range of applicability in terms of particle size, shape, or refractive index. Therefore, it is not surprising that many light-scattering applications [e.g., Ryder et al., 2013], especially those where single scattering is not the central focus (e.g., global climate models), still commonly use scattering data based on spherical particles, even though more accurate models are available. These state-of-the-art modeling approaches for

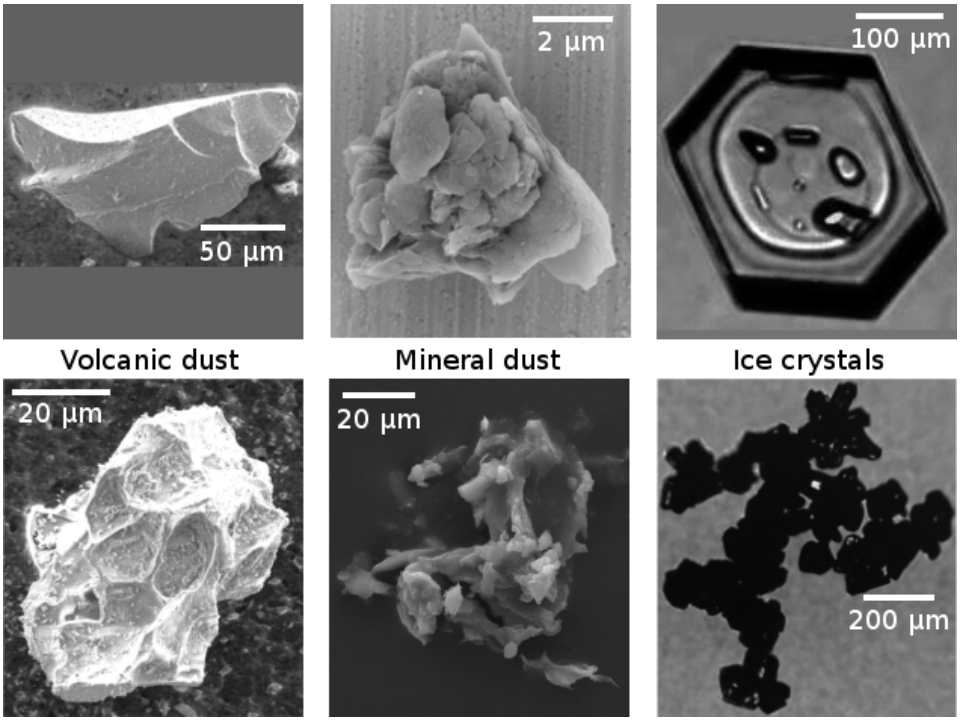


Figure 1.2: Sample volcanic dust (left), mineral dust (middle), and ice crystal particles (right), providing a glimpse of the morphological richness within each category. The images are courtesy of the Amsterdam-Granada light scattering database [Muñoz et al., 2012] (left), Konrad Kandler (middle), and Greg McFarquhar (right).

atmospheric ice crystals and mineral dust particles have been recently reviewed comprehensively by Baran [2012] and Nousiainen and Kandler [2014], respectively. Literature relevant for evaluating the results of the thesis is reviewed in Chapter 5 together with a discussion on the main results.

Throughout the thesis, I strive to combine realistic particle models with available light scattering methods to obtain a realistic representation of the scattering properties of atmospheric particles. The ultimate motivation for such studies originates from the applications that could directly benefit from more accurate scattering models. Two relevant topics are particularly important: the validation of remote-sensing retrievals and the improved accuracy of radiative impact estimations with direct applicability to climate modeling. In fact, selected results of the thesis have already been utilized in such applications; these are discussed more in Chapters 5 and 7.

# 2 Physical properties of atmospheric ice and dust

The physical properties of ice and dust aerosol particles is a broad topic and can be viewed from various perspectives depending on the application. Here, I shortly summarize the key properties of atmospheric ice and dust particles that are relevant for scattering and absorption considerations.

## 2.1 Tropospheric ice crystals

Most atmospheric ice crystals are situated high in the troposphere, 6–10 km altitude, as constituents of high-altitude tropospheric clouds: cirrus, cirrostratus, and cirrocumulus. They are formed by deposition from water vapour, often in heterogeneous nucleation around suitable freezing nuclei such as mineral dust, soot, biological, organic, and ammonium sulfate aerosols [Hoose and Möhler, 2012]. Although ice nucleation is still a topic of ongoing research, a complex but deterministic correlation exists between the habit (i.e., shape class) of the forming crystal and prevailing meteorological conditions, namely temperature and excess vapour pressure over ice [Bailey and Hallett, 2009]. However, different ice crystal habits are not only the result of nucleation and present conditions, but also the previous conditions experienced during crystal growth. Due to the molecular structure of water, ice crystals favor hexagonality, which is macroscopically seen in the crystal images taken by a Cloud Particle Imager (CPI). Since the ice crystals present a continuum of shapes rather than clearly bounded shape classes, it is not straightforward to categorize the habits and, therefore, a varying number of habit classes are identified in the literature. Especially in light-scattering modeling, the number of habit classes considered is typically smaller than in microphysical considerations due to the limited amount of available particle models for scattering; for example, Bailey and Hallett [2009] distinguish around 30 crystal habits, whereas Yang et al. [2013] have constructed a scattering database for 11 habits.

Crystals can grow to centimeters in size in ice clouds before gravitational settling removes them from the environment suitable for crystal growth. In cold climates, the crystals may even grow to snowflakes or reach the surface as single crystals. The observed diameter of the crystals varies from less than 10 $\mu$m from the cloud top to several centimeters toward the cloud bottom [Baran, 2012, and references therein]. Crystal habits vary as a function of diameter; therefore, a size-shape distribution in addition to concentration is necessary for a complete description of ice-cloud crystals in radiative flux computations. Images of crystals smaller than about 50 $\mu$m in diameter suffer from the limited resolution of the CPI instrument and, therefore, their habits cannot be resolved. One modeling scheme is presented in Paper IV; other suggestions have included shapes of droxtals [Yang et al., 2003] and Chebyshev polynomials [Mugnai and Wiscombe, 1980]. The models have been compared by Um and McFarquhar [2011], who also present another particle

model: the budding Bucky ball.

In addition to size and shape, the structure of ice crystals, both internal inhomogeneity and surface structures in the form of roughness, have been recognized as significant factors in scattering [e.g., Sun et al., 2004; Macke et al., 1996]. In practice, little observational *in situ* data of these features are available; however, numerous laboratory measurements of ice crystal analogues exist [e.g., Ulanowski et al., 2006]. The resolution of imaging probes does not reveal small details of the crystals, but data from the Small Ice Detector SID probe [Kaye et al., 2008], which images the scattered intensity instead of the particle, suggest the presence of rough surfaces in ice crystals [Schnaiter et al., 2011].

## 2.2 Mineral dust aerosols

Atmospheric mineral dust originates mainly from large deserts (e.g., Sahara) and other arid regions. The lifetime of suspended dust varies mainly as a function of particle size, and can extend up to several months for the smallest particles, making an intercontinental distribution possible [e.g., Middleton et al., 2001]. Dust is classified into fine and coarse modes according to maximum particle diameter, which varies from submicron to millimeter-sized; the largest of which settle quickly, and their radiative impact is thus confined close to the source area.

Mineral dust particles show a great variety of nonspherical shapes and structures, ranging from compact to aggregates and agglomerates, from rounded to faceted and angular, and from thin and flake-like to equidimensional [Nousiainen and Kandler, 2014]. Similar to ice crystals, small-scale surface roughness is considered a major challenge in mineral dust modeling [Nousiainen, 2009].

The shape of the particles is connected to the constituent mineral species. Most of the common mineral species have fairly similar optical properties with almost negligible absorption at visible wavelengths. But, there are some exceptions, such as hematite: even a small amount of hematite has an impact on the scattering properties of dust particles [e.g., Mishra et al., 2012]. Dust particles can be inhomogeneous, i.e., composed of several mineral species; for example Falkovich et al. [2001] found that only 10% of the particles studied were composed of a single mineral. In Paper VI, energy-dispersive spectroscopy is used to uncover the mineralogical composition of four dust particles, all of which are found to be inhomogeneous; three containing small fractions of strongly absorbing hematite. Mineral dust particles may also become inhomogeneous by mixing with other particulates (e.g., sulfate or water) while aging in the atmosphere.

Lastly, mineral species are typically birefringent, which means that their optical properties depend on the polarization and propagation direction of light. Birefringence is omitted in the modeling considerations of the thesis. Even though certain light-scattering methods are capable of computing scattering by birefringent particles, the direction of the optical axis of the mineral is generally unknown. Luckily, it appears that birefringence may not be a major issue, except possibly for polarimetric and other polarization-sensitive applications and for oriented particles [Nousiainen et al., 2009; Dabrowska et al., 2012, 2013].

## 2.3 Volcanic dust aerosols

Unlike ice crystals and mineral dust particles, the atmospheric concentration of volcanic dust varies enormously according to the frequency and strength of major eruptions. In an eruption, ash is ejected high in the atmosphere where the finest, micrometer-scale particles, called volcanic dust, can stay suspended several months [Rose et al., 2001].

Volcanic-dust shapes are far from spherical and have little resemblance to mineral dust. A visual inspection of scanning-electron microscope images in Muñoz et al. [2004] and Riley et al. [2003] shows the irregularity of the particles produced in the eruption. Riley et al. [2003] classify the particles in three categories according to their shape and structure: vesicular, non-vesicular, and miscellaneous. Vesicular particles have a highly porous internal structure that is also visible on the surface with crater-like features, i.e., vesicles, see Fig. 1.2, bottom left. The vesicular cavities are formed as gas escapes while the volcanic melt cools. Some non-vesicular particles are smooth and compact, as the upper left particle in Fig. 1.2. In fact, some are shattered remains of larger vesicular particles, and are referred to as bubble-wall shards [Heiken and Wohletz, 1985].

The material of volcanic dust is mostly silicate glass that has optical properties close to those of typical, low-absorbing mineral dust species. This raises a question to be answered in Paper II: would it be possible to distinguish volcanic dust from mineral dust based on their light scattering?

# 3 Light scattering

In the atmosphere, electromagnetic radiation constantly interacts with matter on many scales, ranging from molecular scattering to scattering by thick layers of clouds and surfaces such as oceans or deserts. Scattering is so common a process that most of the light that we see in everyday life has been scattered at least once. Traditionally, single scattering is separated from multiple scattering: single scattering is defined as an event where incident radiation is scattered by a single particle; whereas, in multiple scattering, radiation already scattered is incident on yet another particle. Throughout the thesis, I mostly concentrate on elastic single scattering where radiation interacts with a single particle. In Paper V, however, multiple scattering is considered in connection to a cirrus cloud and, therefore, I introduce the relevant single-scattering theory and the basics of radiative transfer.

## 3.1 Theory of single scattering and absorption

Light scattering is fundamentally about the interaction of an electromagnetic field with the electric charges of matter, in most cases mainly electrons. The solution begins from the Maxwell equations that describe the properties of the radiation by relating the electric and magnetic fields together [e.g., Jackson, 1999; Bohren and Huffman, 1983]. The constitutive relations link the fields with the material's electric permittivity and magnetic permeability; the latter is approximately that of the vacuum for non-magnetic materials treated throughout the thesis. Permittivity and permeability are more often presented in the form of a refractive index by a complex number $m$, where $\mathrm{Re}(m)$ is a measure for the phase velocity of the electromagnetic radiation in the material and $\mathrm{Im}(m)$ signifies the absorptivity of the material; for nonabsorbing medium, $\mathrm{Im}(m) = 0$. To link the electromagnetic fields inside and outside the particle, boundary conditions over the interface are necessary. In general, however, the resulting set of equations is not analytically solvable, so approximate numerical methods must be used (see Sect. 3.3).

Instead of the components of the electric and magnetic fields, the properties of light are more conveniently characterized by the Stokes vector $\bar{S} = [I, Q, U, V]$; time integrals of the electric and magnetic fields result in zero values, whereas the elements of the Stokes vector yield meaningful temporal averages and can, therefore, be more easily measured. The first element $I$ denotes the intensity, and $Q$, $U$, and $V$ describe the polarization state of the radiation. Polarization is related to the time-dependent direction in which the electric field $\mathbf{E}$ is oscillating. Far from the particle, the oscillations take place in a plane perpendicular to the direction of wave propagation. In this plane, the basis is described with respect to the scattering plane, and the electric field is characterized with its components parallel ($E_{\parallel}$) and perpendicular ($E_{\perp}$) to this plane. In the case of a simple

harmonic wave, the amplitude of the electric field varies sinusoidally and the field vector traces an ellipse in the plane of oscillation. In this case, radiation is referred to as elliptically polarized. Linear and circular polarization are two special cases of elliptical polarization. In the former, the field components are in phase and the ratio between their amplitudes remains constant, while in the latter, the components have equal amplitudes but a phase difference of $\pi/2$. More specifically [for derivation, see, e.g., Bohren and Huffman, 1983], the Stokes parameter $Q$ represents the difference between horizontally and vertically polarized intensities, $U$ the difference between linear $+\pi/4$ and $-\pi/4$ polarized intensities, and $V$ the difference between right and left circularly polarized intensities, defined as clockwise and counter-clockwise rotation of the electric field vector, respectively. Unpolarized radiation is a mixture of random polarization states; in practice, incident sunlight can be treated as unpolarized radiation. In particular, the treatment of unpolarized radiation is practical with the Stokes parameters because there $Q = U = V = 0$.

In a single-scattering event, the Stokes vectors for the incident (subscript inc) and scattered radiation (sca) are related through a $4 \times 4$ scattering matrix

$$\begin{pmatrix} I_{\text{sca}} \\ Q_{\text{sca}} \\ U_{\text{sca}} \\ V_{\text{sca}} \end{pmatrix} = \frac{1}{k^2 r^2} \begin{pmatrix} S_{11} & S_{12} & S_{13} & S_{14} \\ S_{21} & S_{22} & S_{23} & S_{24} \\ S_{31} & S_{32} & S_{33} & S_{34} \\ S_{41} & S_{42} & S_{43} & S_{44} \end{pmatrix} \begin{pmatrix} I_{\text{inc}} \\ Q_{\text{inc}} \\ U_{\text{inc}} \\ V_{\text{inc}} \end{pmatrix}, \tag{3.1}$$

where $r$ is the distance from the particle and $k$ is the wave number. The scattering matrix $\mathbf{S}$ is a function of the wavelength of light, illumination geometry, and the physical properties of the particle: size, shape, and composition. When averaging over a large amount of single particles in all possible orientations, the dependence of the matrix elements on the illumination geometry is reduced to one angle only: the scattering angle $\theta$ illustrated in Fig. 1.1. The scattering matrix is simplified in special cases, which are presented by van de Hulst [1981]. For an ensemble of randomly oriented particles and an equal amount of their mirror particles, the off-diagonal $2 \times 2$ blocks of the matrix are zero and, out of the eight non-zero matrix elements, only six are independent. For a single particle, as in Paper VI, orientation averaging reduces the number of different matrix elements to ten. An example of four such cases is shown as a function of $\theta$ in Fig. 3.1, which demonstrates that even though the values in the upper right and lower left blocks of the scattering matrix are small, they do slightly deviate from zero.

For unpolarized incident light, $S_{11}$ is proportional to the scattered intensity and $-S_{21}/S_{11}$ is the degree of linear polarization. In the thesis, I especially concentrate on these, but also on the particle's ability to depolarize radiation, which is denoted by the depolarization ratio $D = 1 - S_{22}/S_{11}$. Depolarization means the decrease of the degree of linear polarization and therefore cannot be observed if the incident light is unpolarized; however, it is an essential parameter in active remote sensing, especially for depolarization lidar. Depolarization is connected to the particle nonsphericity and anisotropy [Bohren and Huffman, 1983]: for example, isotropic, spherical particles yield $D = 0$.

For non-absorbing particles, the scattering matrix fully describes the scattering event in the far field. If the particle also absorbs, it is not a sufficient description because part of the electromagnetic energy is transformed into other forms, for example thermal energy. Absorption is quantified by the absorption cross section $C_{\text{abs}}$, which is equal to the area that would be needed to collect the absorbed amount of power from the incident radiation. An equivalent definition applies for the

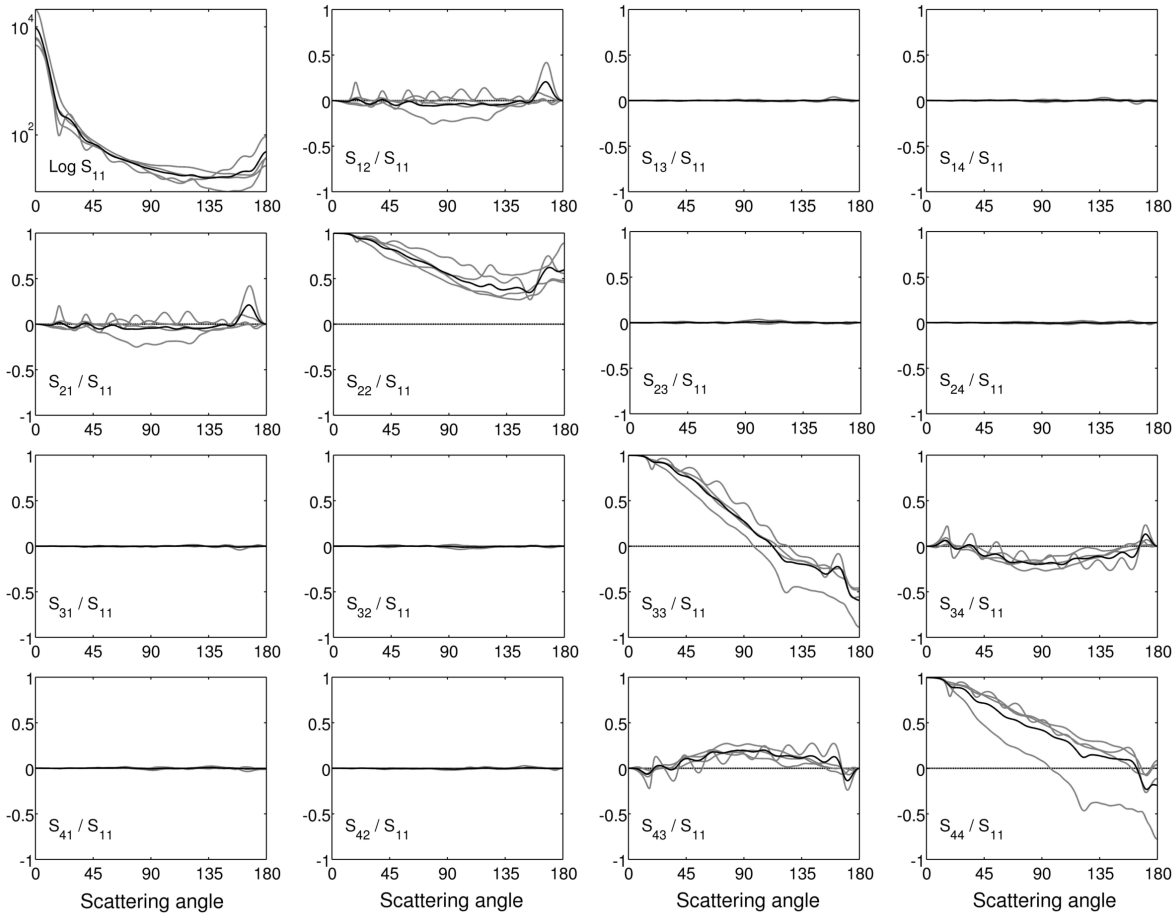


Figure 3.1: All 16 scattering-matrix elements of four orientationally averaged, example mineral dust particles (grey), based on data from Paper VI. Their average is shown with a black line.

scattering cross section $C_{\text{sca}}$ that is proportional to the total scattered power. Together these equal to the total extinction which signifies the total power removed from the incident radiation by the particle; $C_{\text{ext}} = C_{\text{abs}} + C_{\text{sca}}$. The relative contributions of scattering and absorption are usually characterized by the single-scattering albedo $\varpi$ given by

$$\varpi = \frac{C_{\text{sca}}}{C_{\text{ext}}}. \tag{3.2}$$

When the material is nonabsorbing, $\varpi = 1$.

Sometimes, a phase matrix $\mathbf{P}$ is used instead of the scattering matrix $\mathbf{S}$. The two are related as [Bohren and Huffman, 1983]

$$\mathbf{P} = \frac{4\pi}{k^2 C_{\text{sca}}}\mathbf{S}. \tag{3.3}$$

In particular, $P_{11}$ is often referred to as the phase function. The angular distribution of scattered

intensity can be characterized by an integral quantity, the asymmetry parameter $g$, given by

$$g = \frac{1}{2}\int_0^\pi \sin\theta\cos\theta P_{11}(\theta)\mathrm{d}\theta. \tag{3.4}$$

The asymmetry parameter can have values from $-1$ to 1, depending on the amount of radiation scattered into the backward ($\theta > 90°$) and forward ($\theta < 90°$) hemispheres, respectively.

Scattering is not independently dependent on the size of the particle or the wavelength $\lambda$ but, more accurately, on the mutual scale that is defined by a dimensionless size parameter $x = 2\pi a_{\mathrm{eq}}/\lambda$. Here, $a_{\mathrm{eq}}$ is a measure for the particle size which, for nonspherical particles, can be defined as the radius of an equal-volume sphere. The significance of the size parameter should be emphasized because, together with the refractive index, it dictates the whole nature of the scattering event: for small size parameters ($mx \ll 1$) the wavelength of light is much larger than the size of the particle and, therefore, the waves inside the particle are approximately in phase, resulting in scattering similar to that of an ideal point dipole, with little impact due to shape. Then again, for very large $mx$, the phase differences are mostly averaged out in the scattered waves and can be omitted, treating the radiation as rays with no wave nature. The former is called the Rayleigh regime and the latter the ray optics regime. The region in between is called the resonance regime where scattering is dominated by the phase differences of the waves originating from different parts of the particle. Interference of the waves gives rise to many resonant features, both constructive and destructive.

In practical applications, atmospheric particles are an ensemble of particles of different diameters $D$ and shapes $i$. Scattering matrices and cross sections are additive, which makes their averaging straightforward. If the corresponding number $N_{D,i}$ of particles and their single-scattering properties within each size-shape bin (e.g., $g_{D,i}$, $C_{\mathrm{sca},D,i}$) are known, the asymmetry parameter and the single-scattering albedo for an ensemble of particles can be calculated as follows [Macke et al., 1998; McFarquhar et al., 2002]:

$$g = \frac{\sum_D \sum_i g_{D,i} C_{\mathrm{sca},D,i} N_{D,i}}{\sum_D \sum_i C_{\mathrm{sca},D,i} N_{D,i}}, \tag{3.5}$$

$$\varpi = \frac{\sum_D \sum_i C_{\mathrm{sca},D,i} N_{D,i}}{\sum_D \sum_i C_{\mathrm{ext},D,i} N_{D,i}}. \tag{3.6}$$

Averaging tends to smooth resonances in the angular dependence of the scattering matrix elements, as can be seen from Fig. 3.1. Note also, how the upper right and lower left blocks in the figure average around zero.

## 3.2 Radiative transfer

Atmospheric particles scatter and absorb not only the incident solar radiation but also the light scattered by other cloud or aerosol particles, air molecules, and other particulates. This is referred to as multiple scattering. In addition, the solar power incident on different particles varies due to atmospheric extinction. All these processes need to be considered for computing the overall impact of an ice cloud on radiation, as is done in Paper V. To this end, radiative transfer modeling is applied.

A fairly simple plane parallel approximation of radiative transfer is adopted here, meaning that the atmosphere and the cloud within are assumed to be horizontally homogeneous. Thus, it is only necessary to specify the atmospheric and cloud properties as a function of altitude $z$. The atmosphere is divided further into layers within which the properties are assumed to be constant. Averaging over all constituents, e.g. air molecules and cloud particles, within a layer of a thickness d$z$, requires the single-scattering properties $\varpi$, $C_{\text{ext}}$, and $P_{11}$ or $g$. The optical thickness $\tau_z$ of the layer also needs to be specified and can be calculated from the extinction cross section $C_{\text{ext}}$ following

$$\tau_z = \int_{z_1}^{z_2} K_{\text{ext}}(z)\mathrm{d}z, \tag{3.7}$$

$$K_{\text{ext}}(z) = \sum_D \sum_i C_{\text{ext},D,i} N_{D,i}, \tag{3.8}$$

where $z_1$ and $z_2$ are the lower and upper boundaries of the layer, and the volume extinction coefficient $K_{\text{ext}}$ is a measure for the total extinction in a unit volume, and has the unit of inverse length, typically km$^{-1}$.

The radiative transfer equation in the shortwave region, where thermal emission can be ignored, is given for a horizontally homogeneous atmosphere with plane-parallel layers as [Liou, 1980]

$$\mu \frac{\mathrm{d}L_\lambda}{K_{\text{ext}}\mathrm{d}z} = -L_\lambda + \frac{\varpi}{4\pi} \iint P_{11} L_\lambda \mathrm{d}\vartheta \mathrm{d}\varphi, \tag{3.9}$$

where $\vartheta$ and $\varphi$ are the zenith and azimuthal angles in a horizontal coordinate system, $L_\lambda$ denotes the angle-dependent monochromatic radiance, and $\mu = \cos\vartheta$. Note that the phase function $P_{11}(\theta)$ is presented with respect to the direction of incident radiation, i.e., in another coordinate system.

A numerical solution of Eq. (3.9) requires accounting for the relevant boundary conditions at the surface and at the top of the atmosphere, the surface albedo, the solar elevation angle $(90^\circ - \vartheta)$, and vertical profiles of atmospheric composition, including the cloud. The solution gives, e.g., the radiative upward and downward monochromatic fluxes, $F_\lambda^\uparrow$ and $F_\lambda^\downarrow$ respectively, given by

$$F_\lambda^\uparrow = \int_0^{2\pi} \mathrm{d}\varphi \int_0^1 L_\lambda(\mu, \varphi)\mu \mathrm{d}\mu \tag{3.10}$$

$$F_\lambda^\downarrow = \int_0^{2\pi} \mathrm{d}\varphi \int_0^1 L_\lambda(-\mu, \varphi)\mu \mathrm{d}\mu. \tag{3.11}$$

In Fig. 3.2, these fluxes and atmospheric radiative transfer are presented schematically; $F_\lambda^\downarrow$ is the sum of the direct and diffuse downward fluxes, while $F_\lambda^\uparrow$ is the diffuse upward flux. These are calculated in Paper V to demonstrate the impact of the shape distribution of cirrus cloud particles on radiation.

## 3.3 Computational methods

Solving light scattering in a general case implies the use of a suitable numerical method, which is chosen based on the problem at hand. In this chapter, I present all the computational methods

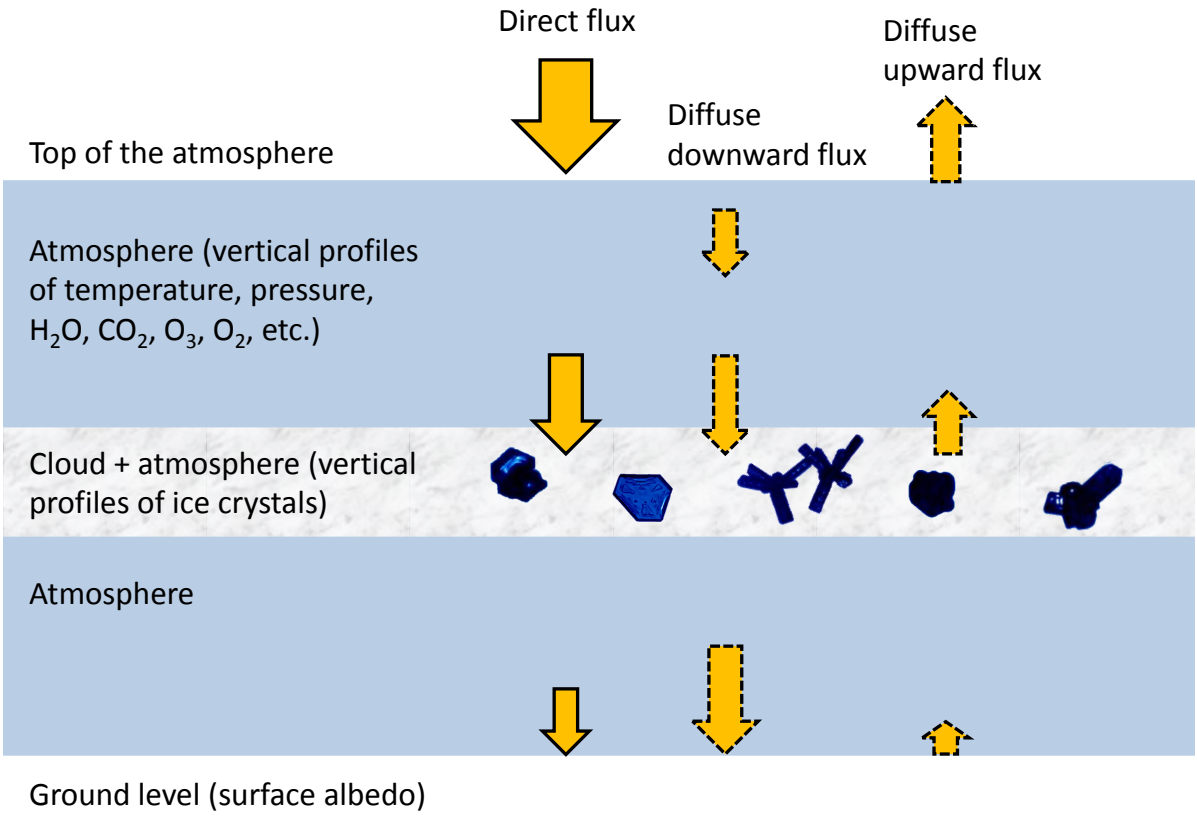


Figure 3.2: A schematic presentation of atmospheric radiative transfer modeling using the plane parallel approximation.

that have been utilized in the thesis for simulating light scattering [for a comprehensive review of light-scattering methods, see, e.g., Kahnert, 2003]. The radiative transfer approach adapted in Paper V is introduced as well.

### 3.3.1 Lorenz-Mie theory

The Lorenz-Mie theory provides an exact, analytical solution for how a homogeneous, isotropic sphere interacts with electromagnetic radiation. The theory solves the vector wave equations in spherical coordinates by describing the electromagnetic field with series expansions of vector spherical wave functions. Therefore, computational methods are not needed to solve the light scattering properties; only the analytical solution needs to be evaluated. The theory was originally independently formulated by Lorenz [1890], Love [1899], Mie [1908], and Debye [1909]. Its derivation is shown with a modern formulation by, e.g., Bohren and Huffman [1983] who also provide the reader with a Fortran 77 version of the computational code. In the thesis, computations of scattering by spherical particles were made using the code by Mishchenko et al. [2002] which

also incorporates the integration of the single-scattering properties over particle size distributions.

Because of the analytical nature of the solution, it is valid throughout all size parameters and refractive indices, only requiring a higher number of series expansion terms to be incorporated at large size parameters to obtain convergence. Computational times are, typically, fractions of a second, which is one of the obvious reasons for its widespread use.

### 3.3.2 *T*-matrix method

The *T*-matrix method can be considered an extension of the Lorenz-Mie theory: it applies a similar approach to nonspherical particles. The electromagnetic fields are, again, described by series expansions of vector spherical wave functions, and the *T*-matrix is used to transform the expansion coefficients of the incident field into the coefficients of the scattered field. The *T*-matrix is derived from the boundary conditions at the interface, which relate the incident field to the internal field and, ultimately, to the scattered field. The method was initially formulated by Waterman [1965] and has later been developed further. In particular, Mishchenko [1991] introduced an analytical averaging over orientations and Mishchenko and Travis [1994] extended the computational precision of the method to cover larger size parameters. Moreover, Laitinen and Lumme [1998], Havemann and Baran [2001], and Kahnert et al. [2001] applied the *T*-matrix method for non-axisymmetric particles.

The shape of the particle surface is accounted for through the boundary conditions. Therefore, only star-like geometries, where the surface can be expressed as an unambiguous function of the angles of the spherical coordinate system, are feasible. The computations are significantly faster for particles with symmetries, for example spheroids, finite circular cylinders, and Chebyshev particles. In the thesis, the *T*-matrix code by Mishchenko and Travis [1998] has been utilized in Papers III and VI to compute scattering by spheroidal particles.

### 3.3.3 Discrete-dipole approximation

Whereas methods based on the Lorenz-Mie theory and the *T*-matrix formalism are based on surface integrals, the discrete-dipole approximation (DDA) is an example of a method requiring volume integration. It was originally introduced by Purcell and Pennypacker [1973]. In the DDA, the particle is considered as a collection of small volume elements, called dipoles. The electric field induced on each dipole results from the superposition of the incident field and the fields induced by all other dipoles. In the calculation of the scattered field far from the particle, the electric field induced on each dipole is weighed by the polarizability of the dipole before an integration over the entire volume of dipoles. The dipole polarizability is connected to the macroscopic refractive index. This connection can be established through several approaches; the one used in the DDA computations of the thesis is called the lattice dispersion relation (LDR), which requires that an infinite lattice of points with a polarizability $\alpha$ should have the same dispersion relation as the macroscopic material that the dipoles are representing [Draine and Goodman, 1993].

Despite the name, the DDA is not an approximation but an exact solution to the scattering by a collection of point dipoles. What is approximated in the method, is the polarizability of the dipoles and the geometry of the particle through volume discretization. For a sufficiently accurate representation of the particle, the interdipole separation $d$ should be small compared to

any structural lengths of the particle and to the refracted wavelength. According to numerical studies [Draine and Flatau, 1994], the latter criterion is sufficiently satisfied if 10 dipoles are used per wavelength in the medium. Later, Draine and Flatau [2009] have specified that even smaller dipole size corresponding to

$$|m|kd < 0.5 \tag{3.12}$$

is needed especially when considering differential scattering quantities, such as the scattering-matrix elements. Similar results are reported in the review by Yurkin and Hoekstra [2007], who nevertheless conclude that a suitable criterion depends much on the application. For integrated quantities, such as the asymmetry parameter or the single-scattering albedo, it is generally accepted that a more relaxed condition can be used [Draine and Flatau, 1994]:

$$|m|kd \leq 1.0. \tag{3.13}$$

It has been pointed out by Zubko et al. [2010] that the criterion in Eq. (3.12) is generally too restrictive. Zubko et al. [2010] showed that, for irregular particles averaged over orientations, the criterion in Eq. (3.13) leads to sufficiently accurate scattering matrices. Paper VI found this to be correct for $S_{11}$ and $-S_{12}/S_{11}$; however, $S_{44}/S_{11}$ and $S_{22}/S_{11}$ appeared to be more sensitive to the discretization.

In addition to the criteria for $d$, the accuracy of the DDA deteriorates with increasing refractive indices. In general, an adequate accuracy is achieved when

$$|m-1| < 2. \tag{3.14}$$

Because of its applicability to arbitrary shapes and inhomogeneous compositions, the DDA has been the main computational method in Papers I, II, and VI. The publicly available DDA codes ADDA [Yurkin and Hoekstra, 2011] and DDSCAT [Draine and Flatau, 2009] have both been utilized in the thesis.

### 3.3.4 Ray optics with diffuse and specular interactions

Traditional ray-optics approximation is a truly approximate light scattering method where the wave nature of light has been omitted, and the approximation is, therefore, only reasonable for particles much larger than the wavelength. The solution is a combination of diffraction and geometric-optics approximation; the latter means that radiation propagates as rays, and scattering is modeled as a sequence of specular Fresnellian reflection and refraction phenomena on the surface. An improvement to this has been introduced by Muinonen et al. [2009] in their ray optics with diffuse and specular interactions (RODS) model, where the traditional approach of Monte Carlo ray tracing has been combined with a radiative transfer scheme to incorporate diffuse scattering on the surface or inside the particle.

The diffuse scatterers are characterized by their single-scattering albedo and scattering matrix. The scattering matrix can be entirely user-defined [as in Nousiainen et al., 2011b] or, as in Paper IV, specified using a semi-empirical double Henyey-Greenstein matrix that is defined by four parameters: the total asymmetry parameter, the forward and backward asymmetries, and a parameter for the maximum polarization. In the case of internal diffuse scatterers, the length of

the mean free path is also specified. External diffuse scatterers are considered a plane-parallel surface layer described by the optical thickness. Sensitivity studies of the impact of these parameters show that scattering can be greatly affected especially by the choice of the mean free path or optical thickness [Muinonen et al., 2009].

Internal scatterers can be interpreted as a model for particle inhomogeneity. In Paper IV, RODS is utilized for modeling the impact of air inclusions inside ice crystals. The approach with external diffuse scatterers can be interpreted as an approximate way of considering small-scale roughness on the surfaces of particles much larger than the wavelength, such as large mineral dust particles [Nousiainen et al., 2011b].

### 3.3.5 Radiative transfer approach DISORT

DISORT is a radiative transfer algorithm designed for a plane-parallel medium of multiple layers by Stamnes et al. [1988]. The program is part of the publicly available radiative transfer package libRadtran [Mayer and Kylling, 2005].

DISORT computes the radiances and fluxes for monochromatic, unpolarized radiation in a medium that can have a vertical structure and temperature profile but is horizontally homogeneous. For an ice cloud, scattering and absorption are determined by $g$, $\varpi$, $C_{\text{ext}}$, and $N$. Other physical processes included in the approach are bidirectional reflection at the surface and Planckian thermal emission. This method is used in Paper V to determine the impact of different ice crystal shape distributions to the shortwave radiative fluxes of a vertical atmospheric profile including an ice cloud. Molecular scattering and absorption is accounted for using a U.S. standard atmosphere in the computations [Anderson et al., 1986].

# 4 Particle modeling

Modeling atmospheric ice crystals, mineral dust, and volcanic dust for light scattering purposes is an interesting and demanding task for two reasons. First, as described in Chapter 2, the atmosphere is extremely rich in particle sizes, shapes, structures, and compositions. The models introduced in this chapter only cover a fraction of the particle types encountered in the atmosphere. Nevertheless, they offer innovative solutions that are also applicable elsewhere. Second, the models need to be designed with respect to the available computational light scattering methods that have their own restrictions regarding the physical properties that can be considered. In what follows, I shortly introduce the particle models developed or applied in the thesis; they are illustrated in Fig. 4.1.

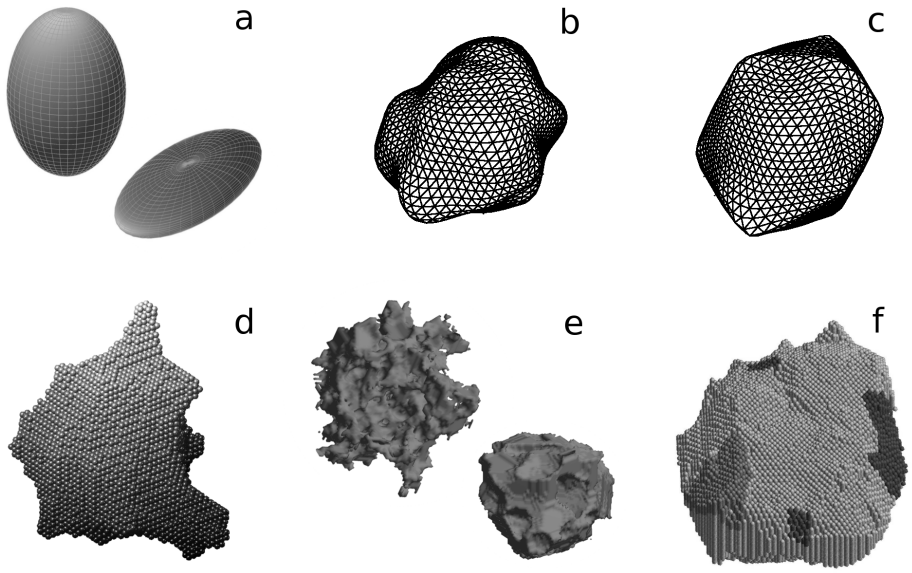


Figure 4.1: Particle models developed or applied in the thesis: a) oblate and prolate spheroids, b) Gaussian random sphere, c) convex-hull-transformed Gaussian random sphere with emphasized sixfold symmetry, d) concave-hull-transformed aggregate of spheres, e) porous volcanic dust model with small and large vesicles, and f) inhomogeneous stereogrammetric shape.

## 4.1 Shape distribution of spheroids

Spheroids are a first improvement when shifting from spherical to nonspherical particles and, yet, they have proven to be quite successful in modeling scattering by more irregular shapes. By definition, a spheroid is obtained by rotating an ellipse about its major or minor axis, which result in a prolate or an oblate spheroid, respectively. A spherical shape is obtained as a special case. Spheroids are characterized by their aspect ratio $\epsilon = a/b$, where $b$ is the dimension along the spheroid's axis of symmetry and $a$ is the dimension perpendicular to the symmetry axis. Hence, $\epsilon < 1$ corresponds to prolate spheroids while $\epsilon > 1$ for oblate shapes. Oblate and prolate spheroids are, however, more conveniently compared by defining a shape parameter $\xi$ similar to the conventions of Paper III, Nousiainen et al. [2006], and Kahnert et al. [2002]:

$$\xi = 1 - \frac{1}{\epsilon}, \quad \epsilon < 1 \quad \text{(prolate)} \tag{4.1}$$

$$\xi = \epsilon - 1, \quad \epsilon \geq 1 \quad \text{(oblate)}. \tag{4.2}$$

This way, oblate spheroids have $\xi > 0$, spheres $\xi = 0$, and prolate spheroids $\xi < 0$, and in both oblate and prolate cases, elongation is linearly proportional to $\xi$.

The shape distribution of spheroids is a distribution of aspect ratios defined with $\xi$. Because of the inherent computational limitations of the *T*-matrix method, extremely elongated shapes are not considered but the shape distribution is, in Paper III, limited to shapes between $-1.8 \leq \xi \leq 1.8$ with intervals of 0.2.

In Paper III, we search for an optimal shape distribution of spheroids for the best possible fit to the laboratory-measured mineral dust scattering matrices. The optimization is performed through nonlinear fitting using the Levenberg-Marquardt method. The method requires an initial shape distribution and, since previous studies [e.g., Nousiainen and Vermeulen, 2003; Kahnert, 2004; Nousiainen et al., 2006; Dubovik et al., 2006] have agreed that spheroids with high aspect ratios are needed to successfully reproduce scattering by mineral dust particles, the shape distribution is initially parametrized according to the following power-law

$$p(\xi) = C|\xi|^n \tag{4.3}$$

where $C$ is a normalization constant and $n$ is the power-law index ($n \geq 0$).

## 4.2 Gaussian random sphere

The Gaussian random sphere is a stochastic shape model based on deforming a spherical surface in a statistically controlled manner. The model has its roots in the light-scattering studies of stochastically shaped particles by Peltoniemi et al. [1989]. Based on this, the concept of the Gaussian random sphere was then introduced by Muinonen et al. [1996] who first applied it to scattering by particles much larger than the wavelength and later to wavelength-scale particles [Muinonen et al., 2007]. In the thesis, the Gaussian random sphere geometry has been used in Papers I, II, IV, and VI.

The surface of a Gaussian random sphere is defined in a spherical coordinate system by $\mathbf{r} = r(\vartheta, \phi)\mathbf{e}_\mathrm{r}$. Let the average radius of the particle be $a$ and $\sigma$ the relative standard deviation of this

radius. A varying surface with hills and valleys is generated by the spherical-harmonics series $s$:

$$\mathbf{r} = \frac{a \exp[s(\vartheta, \phi)]}{\sqrt{1+\sigma^2}} \mathbf{e}_\mathrm{r}, \tag{4.4}$$

$$s(\vartheta, \phi) = \sum_{l=0}^{\infty} \sum_{m=-l}^{l} s_{lm} Y_{lm}(\vartheta, \phi), \tag{4.5}$$

where $Y_{lm}$ are Laplace's spherical-harmonics functions and $s_{lm}$ are complex weights, with real and imaginary parts as Gaussian random variables with zero means. The Gaussian random spheres are by definition star-like, i.e., for each point $(\vartheta, \phi)$ there is only one value of $r$. Individual realizations are generated by setting the weights $s_{lm}$ using statistics specified by the covariance function of radius. This covariance function, denoted by $\Sigma_s(\gamma)$ with $\gamma$ determining the angular distance between two directions, can be represented as a series in Legendre polynomials $P_l$:

$$\Sigma_s(\gamma) = \sum_{l=0}^{\infty} C_l P_l(\cos\gamma). \tag{4.6}$$

Here, the coefficients for the different degrees $l$ are $C_l \geq 0$. The sum of the coefficients is related to the standard deviation of the radial distance:

$$\sum_{l=0}^{\infty} C_l = \ln(1+\sigma^2). \tag{4.7}$$

In practice, the series expansion is truncated at some $l_\mathrm{max}$; in the thesis, I used $l_\mathrm{max} = 10$ or $l_\mathrm{max} = 15$, depending on the application. Coefficients of the degrees $l = 0$ and $l = 1$ are not related to the actual shape and are therefore often set to zero. In some applications, the coefficients are further parametrized by a power-law covariance function with a power-law index $\nu$ and a normalization constant $C$:

$$C_l = \frac{C}{l^\nu}, \quad l = 2, 3, \ldots, l_\mathrm{max}, \tag{4.8}$$

such that $\sum C_l = 1$. With the power-law covariance function, the Gaussian random sphere is a function of two parameters only: $\sigma$ and $\nu$.

In Paper IV, the coefficients of the Legendre polynomials were manipulated to enhance the sixfold symmetry of a Gaussian random sphere. First, the $C_6$ coefficient was increased 50-fold and, finally, all coefficients were set to $C_l = 0$, except for $C_6 = 1$.

A program for generating the Gaussian random sphere geometry has originally been implemented by Karri Muinonen and Timo Nousiainen; in the thesis, I used it but also wrote a new Fortran 95 adaptation of the program.

## 4.3 Concave-hull transformation

The concave-hull transformation is a method for defining a surface around an arbitrary particle or a group of particles. This method is first presented in Paper I where it is applied to Gaussian random spheres and aggregates of spheres. The method is also demonstrated for the generation

of inhomogeneous particles with concave coatings. Concave-hull transformation has also been utilized in Paper II as a boundary surface when generating porous, cratered particles. Papers IV and V use the convex hull, which is the special case of a concave hull.

The concave hull for an arbitrary shape is generated by rolling a sphere over the shape considered: the inner surface formed by the rolling sphere determines the concave hull. The only parameter controlling the shape of the hull is the scale radius $h = R/a_{\mathrm{eq}}$, which relates the radius of the sphere $R$ to the equal-volume sphere radius $a_{\mathrm{eq}}$ of the original shape considered. Convex parts of the shape remain, naturally, unchanged in this transformation but concavities are affected: when $h \to 0$, the concave hull approaches the initial shape while, for $h \to \infty$, a convex hull, where a tangent never crosses the surface, is obtained.

Numerically, the algorithm for computing the concave hull can be made in two ways. For arbitrary shapes, a volumetric approach described and applied in Paper I for aggregates of spheres is recommended but, since it can be computationally heavy, a less demanding ballistic approach can be adapted in the special case of star-like particles, such as the Gaussian random spheres.

## 4.4 Stereogrammetric shapes

Stereogrammetry is a well-established method for the retrieval of a surface from a stereo pair of images. In Paper VI, the method is used for retrieving the surfaces of individual, micrometer-sized mineral dust particles directly from a stereo pair of scanning-electron microscope images. In that respect, the stereogrammetric shapes are fundamentally different from the other shape modeling methods of this chapter: they are not based on any mathematical shape model but on the true shapes of the dust particles.

A detailed description of the retrieval of corresponding point coordinates between the two images is provided in Paper VI. Currently, the method works well only if the tilting angle separation between the two images is small enough, which implies that, in practice, stereogrammetrically retrieved surface is obtained from roughly only one half of the particle. For the construction of the missing part, two approaches are used: full mirroring or scaled mirroring. In both approaches, the height $h$ or the aspect ratio of the particle is not changed. The difference is that in full mirroring, every point for which $z < 0.5h$ is deleted and the lower hemisphere is mirrored from the upper hemisphere. In scaled mirroring, only the space between the lowest observed points and the stage is obtained by a mirrored surface, which is then scaled to fit the remaining space.

The discrete-dipole approximation is chosen as the most appropriate method for these light-scattering computations; thus, the stereogrammetric shapes are volume-discretized. Resolution of the triangulated surface resulting from stereogrammetry is generally very good but loses accuracy at the edges of the image. In practice, the resolution of the volumetric discretization dictates how well small-scale details can be represented by the model.

The largest limitation of this method is its inherent inability to retrieve the internal structure of a particle. When considering, e.g., porous or aggregated particles, other methods are needed. For example, in Paper VI, the volume-discretized version of the stereogrammetric shape is made inhomogeneous by changing the refractive indices of selected dipoles.

## 4.5 Internal structure

Atmospheric particles can possess various types of internal structure, such as inhomogeneity or porosity, on many scales. The challenge in its modeling is that little information of internal structure is available. When suitable measurements are not available, the studies can be considered sensitivity studies. In the thesis, essentially four different modeling approaches of internal structure are used in Papers I, II, IV, and VI.

The concave-hull transformation described in Sect. 4.3 can be conveniently used for modeling inhomogeneity in the form of a coating, where the original particle is composed of a different material than what is used for the volume between the hull and original surface. This method is applicable only for volume-integral methods such as the DDA.

Porous volcanic dust particles in Paper II are an application of the concave-hull coating. The particle generation begins with a ballistic cluster of spheres and its concave-hull transformation. However, now the spheres are selected as empty space and the concave-hull coating is taken to represent the dust material. The spheres are replaced with Gaussian random spheres to generate nonsphericity in the cavities, which causes the cavities to merge, to some extent. An analogous way of creating porous spheroids has subsequently been applied by Nousiainen et al. [2011a].

In applications of the traditional ray-optics approximation, internal structure is omitted because the scattering solution is obtained through a surface representation of the particle, instead of volume. In the RODS modification [Muinonen et al., 2009] though, internal structure can be considered as diffuse, internal scatterers defined by their characteristic single-scattering properties and quantified by specifying a length for the mean free path. This method is applicable for studying the impact of diffuse internal structure, such as small air inclusions inside ice crystals in Paper IV, but is unlikely to be suitable for modeling macroscopic inhomogeneity or high porosity.

Internal inhomogeneity of mineral dust particles is, for the first time, realistically distributed and modeled in Paper VI along with a realistic shape for the model particles. Measurements with energy-dispersive spectroscopy show the elemental distribution within the particle. When combined with an analysis of the visible surface morphology, the mineralogical composition can be derived. The inhomogeneities were incorporated in the volume-discretized model by changing the refractive index of selected dipoles. Assumptions are made regarding the exact depth of the inhomogeneities, because that could not be retrieved by spectroscopy. Possible birefringence of the minerals is omitted because of the lack of knowledge of the optical axis directions in each mineral.

The distribution of material inhomogeneity is often assumed isotropic in light-scattering studies, and leads to the use of effective-medium approximations where one refractive index is used to model the full range of materials in the particle. These approximations have been reviewed by Chýlek et al. [2000]. In Paper VI, an effective refractive index $m_{\text{eff}}$ is derived for each of the particles as a volume average of the permittivities of the mineral components to test the applicability of the method in that particular case.

## 4.6 Ice-crystal classification with principal component analysis

Compared to the other methods presented in this chapter, this one is not a method for creating new particle models. Instead, I consider the Ice-crystal Classification with Principal Component Analysis (IC-PCA), which is a tool for the classification of two-dimensional shapes specially designed for ice crystal silhouettes obtained from CPI image data. Background of the development of the IC-PCA is available in Paper V; here, I only summarize the general logic of the method.

The classification is built on training data acquired from selected CPI images of crystals of the arctic, midlatitude, and tropical ice clouds. Eight habits (i.e., shape classes) are identified for crystals with a maximum diameter $D \geq 100$ $\mu$m: plate, bullet, column, irregular, plate aggregate, column aggregate, bullet rosette, and bullet-rosette aggregate, see Fig. 4.2. The first four habits are categorized as compact and the last four as non-compact habits. As the training data for each habit class, 150 representative images have been manually selected, 50 from each latitude. Their extracted perimeters have then been described by parameters that are most appropriate for habit separation. These parameters are related to: 1) the area of the silhouette, 2) the aspect ratio, 3) correlations in the perimeter shape, and 4) detected corners in the perimeter. In total, 29 parameters are used, 19 of them for compact and 26 for non-compact crystals. Due to the large amount of dimensions, a standard technique for dimension reduction, called the principal component analysis [PCA; e.g., Webb and Copsey, 2011], has been applied. With PCA, the data is transformed into a coordinate system where the axes are directed along the largest correlations between the parameters and, if desired, the dimensions with the least significant correlation can be omitted. In IC-PCA, two dimensions are excluded for both compact and non-compact crystals to optimize the classification performance (see Paper V for details).

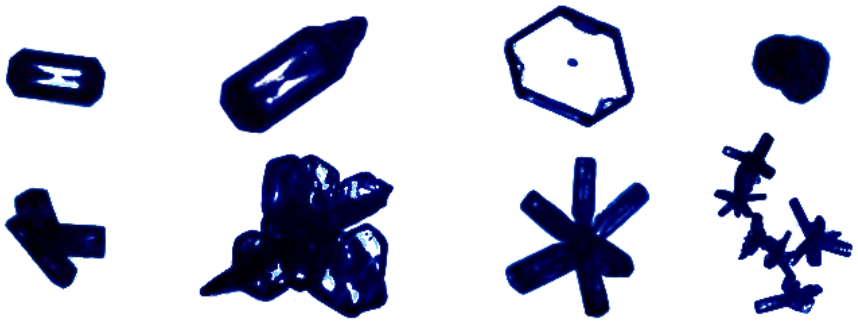

Figure 4.2: Example crystals of the eight habit classes of the IC-PCA. The compact habits are in the upper row: column, bullet, plate, and irregular. Non-compact habits are shown in the lower row: column aggregate, plate aggregate, rosette, and rosette aggregate.

The classification for a new crystal image is fully automated and proceeds as follows:

- The perimeter of the crystal is extracted from the image.
- Parameters describing the area, aspect ratio, shape, and detected corners are computed from the perimeter.
- The crystal is categorized as compact if the number of detected corners is $N_{\text{corner}} < 11$ and if the crystal has a nearly convex shape (i.e., $A/A_{\text{ch}} > 0.9$, where $A$ is the area of the

silhouette and $A_{ch}$ is the area inside the convex hull of the detected perimeter). Otherwise, it is categorized as a non-compact crystal.
- The crystal parameters are transformed to the appropriate PCA coordinate system according to its category (compact/non-compact).
- The crystal is classified according to the classes of its five nearest neighbors in the principal component space.

By repeating this procedure for all crystals of one data set, a habit distribution is obtained. The current version of the IC-PCA is written for Matlab due to its combined image processing and computational capability. After the optimization of the code performed by Master's student Jussi Tiira working under my co-supervision, the processing and classification of 1000 CPI images takes 37 seconds of CPU time on a standard laptop processor.

# 5 Discussion

The results of the thesis presented in detail in Papers I–VI contribute in multiple ways to the research on atmospheric ice and dust particles, and their single scattering. Three main themes can be clearly distinguished and are categorized under the following topics: 1) advances in shape modeling, 2) particle inhomogeneity and its impact on scattering, and 3) shape classification. This chapter is devoted to the evaluation of the new findings and progress made within these themes by comparison with related research and applications, if available. Because the thesis is theoretical and modeling-oriented, while closely related to naturally-occurring phenomena, I considered it appropriate to also dedicate special attention to the validation of the results. This is done by briefly reviewing the related efforts made in the thesis in addition to the currently available possibilities for validation.

## 5.1 Advances in shape modeling

It is generally acknowledged that the shape of a particle can have a large impact on the properties of scattered light and, therefore, research in the field has largely concentrated on developing more appropriate shape models, in addition to light scattering methods, for the problems at hand. Because computational methods for scattering by arbitrarily shaped particles are already available, it would be irrational not to take full advantage of those and apply them to shapes that are as descriptive of the real targets as possible; at least when sufficient computational resources are available. Indeed, shape modeling of real-like particles, and validation of simplified models in the same context, have been central themes throughout the thesis.

The concave-hull transformation presented in Paper I is a general methodology for modifying the shape of an arbitrary particle. With only one parameter, it generalizes the concept of the convex hull and is easy to apply. In the thesis, it was utilized in Paper II for creating an outer boundary surface for the volcanic dust models. Other related uses can be envisaged: the concave hull could be an ideal theoretical method for determining the porosity, or packing density, of a porous particle. In a porous medium where porosity is continuous and reaches the surface, the volume of the particle (including the volume of the cavities) is not clearly defined. Porosity is sometimes indicated with respect to the radius or volume of a circumscribing sphere [e.g., Min et al., 2006], which can lead to misleadingly large fractions of empty space compared to that occupied by the material; a two-dimensional example of this is illustrated in Fig. 5.1. Moreover, concave-hull-transformed clusters of spheres are suitable models for aged black carbon aggregates in the atmosphere. As such particles age, their appearance changes, partially due to the bridging effect between the monomers. These particles have been previously modeled using overlapping

spheres and a 3D level-set function for the necking between the monomers [Bescond et al., 2013]. The concave-hull transformation shares some features with another generalization of the convex hull, called the $\alpha$-shapes [Edelsbrunner et al., 1983]. These shapes are used to define a shape for a finite set of point in two or three dimensions with piecewise linear curves.

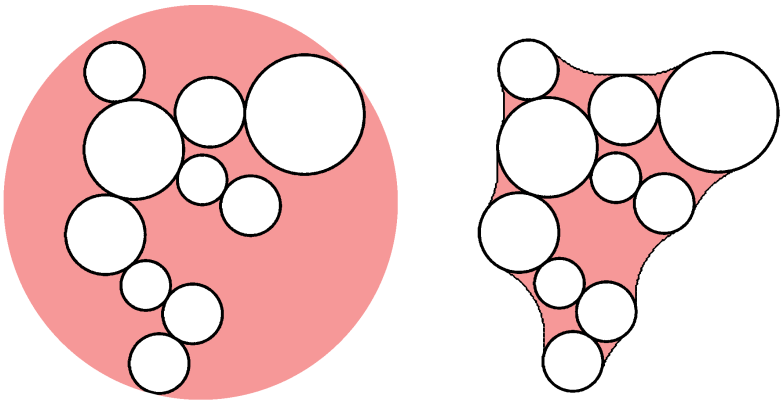

Figure 5.1: Two-dimensional cluster of circles with a circumscribing circle (left) and the same cluster with a concave hull using a scale radius of $h = 0.7$ (right). The shaded area represents the empty space when using the corresponding boundaries to define particle porosity (or packing density).

The model developed for porous volcanic dust particles in Paper II is the first model to realistically mimic their porous internal structure. Previous models for volcanic dust have included spheres [e.g., Niemeier et al., 2009], spheroids [Krotkov et al., 1999], and nonsymmetric hexahedra [Bi et al., 2010], making the model in Paper II quite advanced given its realistic appearance and the level of detail. Paper II concentrates on porous particles, although compact particles are also present in the volcanic dust emissions. The compact particles are considered, in fact, to be fragments of larger porous structures and are referred to as bubble-wall shards, implying that the model in Paper II could, in fact, be applied also to their modeling if the particles were made in larger scales and then broken to form fragments. The motivation for phenomenologically detailed models lies in the desire to obtain more accurate scattering results without the challenges of a realistic, physically based shape model. Such models were achieved in Paper II, resulting in a discovery of the possibility to remotely distinguish porous volcanic dust from mineral dust using depolarization lidar. This model has already been used in a comparative study where the infrared signature of different volcanic dust models are evaluated [Kylling et al., 2013]. Because of their high porosity, real volcanic dust particles are also used as a natural proxy for cometary dust in laboratory measurements, e.g., in the PROGRA2 (Propriétés Optiques des Grains Astronomiques et Atmosphériques) microgravity experiments [Worms et al., 1999]; therefore, the shape model introduced in Paper II could prove very promising to model light scattering by cometary dust and, possibly, help explain little understood scattering phenomena observed in the innermost coma of a comet [Levasseur-Regourd et al., 2013].

A related application of the concave hull is presented in Paper IV, where the statistics for three-dimensional shapes were retrieved from the silhouettes of small ice crystals. Due to diffraction and

the limited resolution of the CPI instrument, the interpretation of the true shape from the silhouette can be ambiguous and, therefore, the impact of minor shape modifications of the retrieved shape on light scattering were tested. These modifications included enhancing the sixfold symmetry by manipulating the Gaussian random sphere Legendre coefficients and adding a convex hull to the surface to form facets. Figure 5.2 demonstrates the ambiguity of crystal shape for the case of low resolution and blurring. Although these modifications were minor, they are seen to produce a 4% increase in the asymmetry parameter. In the literature, other shape models for the small ice crystals have been suggested, and their single-scattering properties are compared by Um and McFarquhar [2011]. Unfortunately, the real shapes of these small crystals cannot currently be observed, so the most suitable model for them cannot be chosen. The situation is evolving however, with new microphysical probes, such as the Small Ice Detector (SID) probe [Kaye et al., 2008], which measures scattering patterns instead of imaging crystals. It may be possible to invert shapes from these measurements, once the appropriate algorithms have been developed. Various model shapes are naturally necessary to solve the inverse problem, and it will be interesting to see whether any of these models can *per se* explain the observed scattering patterns. It is possible, for example, that internal inhomogeneity or surface roughness must also be considered. At least based on Paper IV, internal inhomogeneity can have a larger impact on scattering than the minor shape modifications considered (see Sect. 5.2).

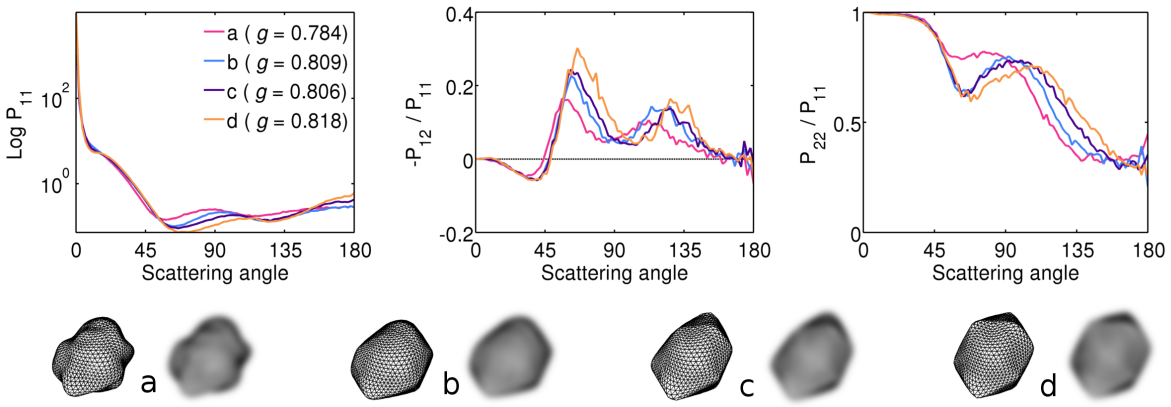


Figure 5.2: Shape modeling of small ice crystals demonstrated with a Gaussian random sphere (a) and its modified versions of an added convex hull (b) and enhanced sixfold symmetry with a convex hull (c, d). To demonstrate the ambiguity of the blurred shape due to low resolution and diffraction, the model images are blurred with image-processing tools. Scattering by particles a-d computed with the ray-optics approximation is also presented.

Regarding the advances taken in the shape and scattering models of mineral dust, Papers III and VI together nicely cover an entire story of the current state of the art. Since proven by Nousiainen and Vermeulen [2003] that the measured scattering matrices of mineral dust ensembles, in that case small feldspar particles, could be reproduced well using a shape distribution of spheroids, the use of spheroids as models for mineral dust has become common practice in numerous studies and remote sensing retrievals; even though the spheroids were used as models for mineral dust

already in the 1980's [Hill et al., 1984]. In addition to good agreement with measured scattering, the popularity of the spheroid model is explained by its computational feasibility. With the *T*-matrix method, the computations are fast, if restricted to modest aspect ratios, and can cover a large size parameter range, which is often necessary in practical atmospheric applications. Moreover, the scattering database of spheroids compiled by Dubovik et al. [2006] has greatly facilitated the use of the model. However, a systematic evaluation of the applicability and performance of the spheroid model was missing until first carried out in Paper III. Fitting the scattering-matrix elements of spheroids to laboratory-measured elements showed that distributions of spheroids can reasonably well reproduce scattering matrices for each of the five dust ensembles considered. Generally, the best fits were obtained using combinations of the most elongated prolate and oblate spheroids. Through critical optimization and assessment, the shape distribution ideal for climate modeling purposes was also suggested. In this study, a profound finding was that different shape distributions of spheroids were optimal for modeling scattering by the same dust type at two different wavelengths, indicating that the spheroidal shapes responsible for the good fits could not be closely related to the shapes of the target particles. This was further confirmed by Nousiainen et al. [2011a], who showed that even scattering by cubes can be reproduced by a suitable distribution of spheroids. Indeed, it was found that the reason why spheroids work so well is that the spheroids form a flexible set for modeling a variety of scattering matrices. As a result, they can provide good fits even if they did not correctly link the particle's physical and single-scattering properties.

There have also been numerous other suggestions as more descriptive models for mineral dust, including concave fractal polyhedra [Liu et al., 2012], Gaussian random sphere [Nousiainen et al., 2011b], irregular rhombohedra [Dabrowska et al., 2013], and agglomerated debris particles [Zubko et al., 2013], to name a few. The performance of different models has been recently evaluated by Nousiainen and Kandler [2014]. What is notable is that even though some of the aforementioned models are phenomenologically similar to dust particles, or include realistic aspects such as accounting for surface roughness, they are all essentially mathematical shape models even though they were based on the shapes of real dust particles. In this regard, Paper VI is fundamentally different. The stereogrammetric modeling method applied to micron-sized mineral dust particles can be viewed as an entirely new approach to realistic light scattering modeling in two ways. First, the shapes are not merely based on real particles but are truly retrieved from the observed topography of the particle surface. Second, it has been common practice to model particle ensembles without considering how individual particles scatter. By establishing the true variability of scattering by individual dust types, modeling of different dust ensembles will become more reliable. In particular, results in Paper VI and Fig. 5.3 show that a sphere, a spheroid, and a Gaussian random sphere are not sufficiently versatile to produce the variability seen in scattering by stereogrammetrically modeled dust particles. In particular, sufficiently high values for $-S_{12}/S_{11}$ and sufficiently low values for $S_{44}/S_{11}$ seem to be challenging to produce with the simplified models.

## 5.2 Particle inhomogeneity and its impact on scattering

While particle shape and its impact on light scattering has been actively studied already for decades, the impact of inhomogeneity has clearly not been given as much emphasis, even though it is a very

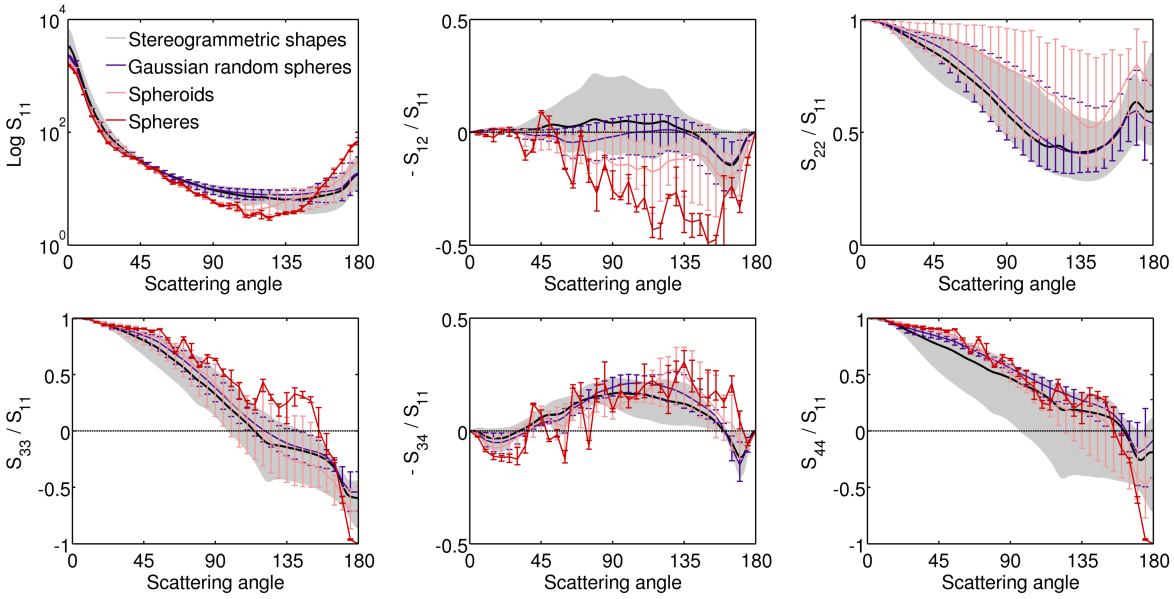


Figure 5.3: Particle-to-particle variation in scattering by different mineral dust models. The particles are presented in more detail in Paper VI.

common feature among naturally-occurring particles. Inhomogeneity can be defined as an internal change in the refractive index; this way, porosity can be interpreted as an extreme type of inhomogeneity. The characteristics of inhomogeneity vary: an agglomerated mineral dust particle or an aged, mixed black carbon particle are good examples of larger scale inhomogeneity, whereas ice crystals or volcanic dust particles with internally mixed, diffuse air bubbles represent a smaller scale of inhomogeneity.

From my point of view, there are two likely reasons behind the lack of studies accounting for inhomogeneity. The first is the (former) lack of suitable computational methods. Scattering by layered spheres can be solved analytically using an extension of the Lorenz-Mie theory but, for inhomogeneous shapes other than spheres, the methods for solving light scattering have become available only recently. For wavelength-scale particles, selected volume-integral methods such as the DDA can be utilized. For particles much larger than the wavelength, arbitrary inhomogeneity cannot be considered by any available method. However, diffuse internal scatterers can be accounted for, e.g., using RODS. Both of these methods — DDA and RODS — have been utilized in this thesis to model different cases of inhomogeneous particles. The second reason is the lack of measured data of the inhomogeneity of atmospheric particles. The lack of measurements tends to lead to the situation where theoretical studies on the subject are more or less sensitivity studies, which can be used to map the potential but not the real effect.

In Paper I, the inhomogeneous mixture of silicate and water ice was studied in the case of wavelength-scale particles. A motivation for this was originally found from Solar-System particles, such as cometary dust, where the suggested composition combination is considered highly plausible. Because a large impact on scattering was discovered, especially related to positive polarization encountered in observations [e.g., Levasseur-Regourd and Hadamcik, 2003] and also in

laboratory measurements [Volten et al., 2001], the topic became one of the central themes in the thesis and is still challenging me to further studies. Paper I presented the concave-hull transformation and studied its impact on scattering by wavelength-scale particles. In addition to considering the shape of the particle, Paper I is the first one to suggest that the model is applicable for studying scattering by inhomogeneous particles and also made the first realizations of these, considering both compact and aggregate particles. The inhomogeneous mixture of silicate and water ice or, more generally, of two substances with different refractive indices, is also relevant for atmospheric particles because of the heterogeneous nucleation of ice around mineral-dust freezing nuclei in the higher troposphere [Hoose and Möhler, 2012], the hygroscopicity of mineral dust in the lower troposphere [Koehler et al., 2009], and mixing of soot with other aerosol components by condensation [Jacobson, 2001]. Also, since a physical model for the collection of inhomogeneities in the grooves and concavities of irregular particles would be very complex to implement, the concave-hull transformation offers a simplistic, yet beautiful, method to model superficial inhomogeneity that differs from a traditional, simplistic coating.

The increase of positive polarization emerges again in the context of porous volcanic ash particles in Paper II. It has been shown that so-called fluffy structures promote positive polarization from scattering by wavelength-scale particles [e.g., Lumme and Rahola, 1994; Nousiainen, 2009] but Paper II systematically showed the significance of the scale of porosity: for two particles with approximately the same packing density, the smaller cavities result in higher positive polarization. The physical mechanism behind this can be explained with the findings of Muinonen et al. [2011] and Tyynelä et al. [2007, 2008] concerning the internal field of the particle. Here, a uniform material allows for the formation of strong resonant structures that decrease the degree of linear polarization, but cavities in the material disturb the formation of these resonances.

If interpreted widely, Paper IV also considers particle inhomogeneity in the sense that the internal scatterers incorporated in the RODS model and applied to irregular ice crystals could model, e.g., internal structure of the ice crystals. However, because little is known on this topic due to the difficulties of observations, this study is more of a sensitivity study parametrized by the scattering properties of the internal scatterers and the mean free path. A striking finding is that the asymmetry parameter can be greatly and systematically decreased by the internal scatterers, resulting in a range of $g = 0.377$–$0.782$, compared to that obtained without the internal scatterers, $g = 0.785$. These findings are in agreement with those reported by Macke et al. [1996], who studied the impact of inclusions on scattering by large ice crystals. The importance of the values reported here can be understood given the estimations of Vogelman and Ackerman [1995], who conclude that the asymmetry parameter should be known to within about 2% or 5% accuracy at cloud optical depths of 12 and 2, respectively, for climate considerations. Based on this, even very small amounts (corresponding to a mean free path of five times the particle radius) of internal scatterers may cause significant inaccuracy in the estimations of the radiative impact of ice clouds.

In all of these studies, the effect of an added inhomogeneity on scattering was examined — added in that sense that scattering was being compared to particles without this feature of inhomogeneity. A different approach to the impact of inhomogeneity can be taken through effective-medium approximations (EMAs). Inhomogeneous particles are often characterized using such approximations to derive one refractive index for the whole particle. These approaches are, by definition, only valid under specific conditions for the inhomogeneity [Chýlek et al., 2000] but are

often applied also outside these conditions. Kahnert et al. [2012, 2013] have recently demonstrated the applicability of EMAs to atmospheric particles where one of the substances is strongly absorbing. They found that large differences can occur, especially for the single-scattering albedo. This is particularly important to consider when modeling aged black carbon particles whose absorption is essential to be correctly accounted for in climate modeling. Certain mineral dust species, such as hematite, are also strongly absorbent. While there have been sensitivity studies on their potential impact on scattering [Longtin et al., 1988; Hu and Sokhi, 2009; Mishra et al., 2012], their distribution has not been realistically considered until Paper VI, where three of the particles included a minor fraction of hematite, 0.7%–2.0% of the total volume. The other, less-absorbing inhomogeneities were also correctly accounted for, although their impact was found to be negligible in the effective-medium comparisons due to the similar refractive indices of the different minerals. For hematite-containing particles, nonsystematic small differences were found in the single-scattering albedo (1% error). Although the differences in the integrated optical properties were not major with low hematite content, the size dependence studies on the angle-dependent scattering-matrix elements gave new insight into the sensitivity of the internal fields to inhomogeneity. Paper VI identified size parameters $3 \leq x \leq 8$ as the most sensitive region to the realistically distributed inhomogeneity, and also that the impact was systematically seen at moderate to large scattering angles. It is possible that the size parameter range depends on the size scale of inhomogeneity, although not necessarily; it is also the area of the strongest resonant features in general.

## 5.3 Morphological classification

Compared to the two previous themes, the classification method for ice crystal silhouettes presented in Paper V might seem odd; however, it also is fundamentally connected to light scattering by ice clouds. In order to compute the radiative impact of an ice cloud, one must first know the single-scattering properties of the ice crystals within. As these depend on the sizes and shapes of the particles, the derivation of the size-shape distribution of ice crystals is the first necessary step towards quantitative estimations of the radiative impact.

Traditionally, the shape distribution of the crystals has been determined, at least partially, manually through a visual inspection and classification of the CPI images. For example, Um [2009] uses a semi-automatic procedure where part of the work has been automated but a manual classification is necessary for 40%–60% of the images. The IC-PCA (Ice-crystal Classification with Principal Component Analysis) classification tool developed in Paper V offers the first fully automatic, objective, and repeatable classification for the input ice crystals. Since previous classification methods have involved a subjective phase, the improvement in efficiency is imminent: the IC-PCA classifies 1000 crystals in only 37 seconds. According to Paper V, preliminary tests on the classification accuracy yielded a success rate of 81.1%. Even though the tests were quite representative with crystals from three different data sets corresponding to arctic, mid-latitude, and tropical ice clouds, further testing would be advisable prior to applying the IC-PCA blindly. An ongoing study aims at a comparison of different classification schemes including the IC-PCA, identifying their strengths and weaknesses, and also paying attention to the different definitions of crystal habits, with the possible and, perhaps, desirable consequence of unifying the conceptions.

Regarding the classification accuracy, the relevant question is whether the IC-PCA is reliable

enough. Because my motivation for developing the classification tool was in computing the size-shape-averaged single-scattering properties for ice clouds, it was necessary not to concentrate on the number 81.1% but to study how the error in classification propagates to the desired application. Hence, the radiative fluxes of the test clouds were estimated in Paper V for both manually and automatically classified CPI data. The shortwave flux differences for both direct and diffuse downward flux at the surface were found to be at most 10%–20% at moderate solar elevation angles. However, it was also discovered that two manual classifications of the same CPI data could result in even larger flux differences. This was a clear indication of the very subjective habit conceptions which would benefit from quantitative criteria for the habits and from an objective, systematic classification.

The IC-PCA is already being applied to collect a habit classification database of ice crystals. Even though estimation of the radiative impact of ice clouds is the application the IC-PCA was designed for, the habit distributions are of interest also for, e.g., determining the ice water content of a cloud and for micrometeorological studies that link the meteorological conditions to the formation of different crystal habits. The methods applied and integrated in the IC-PCA have also been considered promising in other multidisciplinary classification tasks. While developing the IC-PCA, a corresponding method was developed to classify apple silhouettes. It turned out, however, that the apples require an entirely different set of parameters [Hakkarainen, 2011]. Currently, the classification approach of IC-PCA is being adapted to automated identification and classification of space debris from astronomical images, the ultimate motivation being their orbit determination [Virtanen et al., 2013]. Classification after a principal component analysis of retrieved scattering properties could also be tested to improve the classification of different aerosol types from remote sensing retrievals. The current implementation is based on multidimensional cluster analysis [Russell et al., 2010; Cattrall et al., 2005], and optimization of the number of dimensions with the PCA might be worth testing.

## 5.4 Validation

Because a model essentially means a simplified representation of reality, every attempt made for validation of the model is valuable. Validation of a single-scattering model can be made by comparing the simulated scattering matrices to laboratory-measured scattering matrices, as is done in Paper II for volcanic dust and in Paper III for mineral dust. Full scattering matrices have been measured in laboratory for volcanic dust [Muñoz et al., 2004] and various samples of mineral dust species [Volten et al., 2001; Muñoz et al., 2001], and the measurements are publicly available in the Amsterdam-Granada light scattering database [Muñoz et al., 2012].

So far, all the measurements of full scattering matrices are made for particle ensembles. Characterization, however, is much easier for single targets. For scattering by a single particle, possibilities for validating computed results are seen in the SID probe [Kaye et al., 2008], digital holographic imaging [Berg and Videen, 2011], flow cytometers measuring one-dimensional and two-dimensional scattering patterns [Jacobs et al., 2009; Strokotov et al., 2011], and the scattering laboratory at the University of Helsinki, currently under construction.

# 6 Review of papers and the author's contribution

**Paper I** introduces a novel shape modeling method called the concave-hull transformation, which is applicable to any particle shape, and can be used for creating a concave surface that also preserves facets and convex features of the original surface. It can also be applied to create inhomogeneous particles; this is demonstrated with Gaussian random spheres and aggregates of spheres, both of which are coated with another material. Light scattering properties of such wavelength-scale particles are computed using the discrete-dipole approximation, and the results reveal that the polarization by the particles is notably different. A new feature is also identified in the scattering by nonspherical, wavelength-scale particles: depolarization is found to form a double-lobe feature near backscattering.

My contribution was to write a Fortran program for computing the concave hull numerically for aggregates of spheres, while Karri Muinonen coded the transformation for the Gaussian random spheres. I managed all the computations, analyzed the results, and wrote the paper.

**Paper II** presents a stochastic, phenomenological shape model for porous volcanic dust particles. The concave-hull transformation from Paper I is utilized at one stage of the shape generation. The results of the light scattering computations for wavelength-scale volcanic and mineral dust model particles reveal that volcanic dust might be remotely distinguishable from mineral dust by depolarization lidar. Internal porosity is identified to promote positive polarization and decrease the depolarization ratio, and the strength of the effect is found to depend on the scale of porosity. The shape model is validated through a qualitative comparison of scattering by volcanic-dust model particles to the laboratory-measured scattering matrix of a distribution of real volcanic dust particles.

I developed a Fortran program to generate the porous volcanic-dust particle shapes and the corresponding compact particles (that were used as a proxy for mineral dust) with a minor contribution from Evgenij Zubko. Under the supervision of Timo Nousiainen, I carried out all computations and analysis of the results. The text was also my writing, except for the description of the volcanic dust particles (first paragraph of Sect. 3 of the paper) which was written by Olga Muñoz, who also provided the scanning-electron microscope images in Fig. 1.

**Paper III** presents a comprehensive assessment of the applicability of spheroidal particles to the modeling of single scattering by mineral dust particles. Scattering by different shape distributions of spheroids is fitted to the laboratory-measured scattering matrix elements of five different dust samples at two wavelengths to find the best-performing shape distributions for each case. It is found that the optimal distributions are obtained with a large fraction of the most elongated oblate and prolate spheroids and a small fraction of the more equidimensional spheroids. It turns out that spheroids do model the scattering by mineral dust very well but not consistently. For example, different sets of spheroids are needed to model the same sample at two different measurement

wavelengths.

I was responsible for finding the optimal shape distributions of spheroids for each sample through nonlinear fitting, as well as writing Sect. 4.2 of the paper. The power-law fits were performed by Sini Merikallio, who also wrote the majority of the paper. Single-scattering properties of the spheroids were extracted from a pre-computed database.

**Paper IV** investigates light scattering by small irregular ice crystals present in tropical ice clouds. Images of real ice crystals obtained by an aircraft-mounted CPI instrument are used to retrieve the shape statistics of the crystals, and corresponding three-dimensional model particles are generated by modifying the Gaussian random sphere model according to the retrieved crystal shape statistics. Ray-optics computations for the model particles indicate that their asymmetry parameters are larger than those of previously studied midlatitude crystals but that the difference is not sufficiently large to have effects on climate. However, modifications to the shape model show that facets, promoted sixfold symmetry, and in particular internal inhomogeneity can largely change the asymmetry parameter.

My contribution was to conduct the ray-optics computations, implement and study the impact of shape modifications and internal inhomogeneity on scattering, and write the corresponding part of the Results section. In addition, I provided Figs. 3–9.

**Paper V** concentrates on the CPI image data of large ice crystals and develops an automatic classification tool IC-PCA that objectively, efficiently, and fully repeatably classifies the crystal silhouettes. IC-PCA is based on principal component analysis performed on the set of parameters retrieved from the silhouettes. The data are classified into eight habits using both nearest neighbour and Bayesian classifiers, to evaluate their performance. According to preliminary tests on image data from three latitudes, the average classification accuracy of the IC-PCA is 81.1%. The radiative impact of example ice clouds is also estimated for the retrieved habit distributions. This study showed that the errors in the automatic classification result in flux differences not larger than those resulting from two separate, manual classifications.

I was responsible for the majority of the study by implementing the IC-PCA with Matlab (with minor technical contributions from Risto Makkonen and Hanne Hakkarainen), testing it thoroughly, classifying all CPI data, and analyzing the results. The radiative impact of the example clouds was analyzed and the Appendix written in collaboration with Päivi Haapanala, who conducted the radiative transfer computations with libRadtran and provided Fig. A1. Otherwise, the paper was written by me.

**Paper VI** establishes the light scattering properties for four single mineral dust particles by using stereogrammetrically characterized real shapes of the particles. In addition, particle composition is measured with energy-dispersive spectroscopy, and the mineralogical inhomogeneity of the particles is considered in the discrete-dipole approximation computations for wavelength-scale particles. With these elaborate model particles, the natural variability of scattering between different mineral dust types is estimated. Comparisons to scattering by homogeneous, effective-medium particles reveal that the effect of inhomogeneity is size dependent, being the most significant at size parameters from 3 to 8. Simplified model shapes of a sphere, a spheroid, and a Gaussian random sphere did not generally perform well to model the different dust types and scattering quantities considered.

My contribution included selecting the particles used in the study, generating the three-dimensional

model particles based on the stereogrammetric surface coordinates provided by Olli Jokinen, developing modeling schemes for the lower, hidden side of the particle, and defining the compositions for the volume elements according to the mineralogical analysis performed by Konrad Kandler and Dirk Scheuvens. The scattering computations and analyzing the results were my responsibility as well. I wrote the paper, except for Sects. 3 and 4.1, which were written by Konrad Kandler and Olli Jokinen, respectively.

# 7 Conclusions

Ice crystals and mineral and volcanic dust aerosols are important constituents of our atmosphere where they scatter and absorb the solar shortwave radiation and the longwave heat radiation of the Earth. They participate in both local and global meteorology through their radiative properties but also otherwise, e.g., dust as cloud condensation and freezing nuclei, and ice crystals as part of the global water circulation. Knowledge of their single-scattering properties is challenging to establish due to the irregularity and inhomogeneity of the particles but is essential information for accurate estimations of their radiative impact and contribution to global climate, as well as for their characterization through remote sensing. The thesis contributes to this goal by carefully assessing the current, widely used methodology of spheroidal model particles in Paper III; by developing realistic shape models for morphologies of volcanic dust in Paper II, small ice crystals in Paper IV, and mineral dust in Paper VI; by studying the impact of internal structure and inhomogeneity on scattering in Papers I, II, IV, and VI; and by establishing a methodology for an automatic classification of ice crystal shapes in Paper V.

Throughout the thesis, the modeling focus shifts from statistical modeling of ensembles to single particles, and from simplified or phenomenological models to realistic, retrieved shapes, culminating in Paper VI to the presentation of micrometer-scale dust particle models where both the shape and inhomogeneous composition have been directly derived from observations. Interestingly, this is almost opposite to what my own supervisor suggested in his PhD thesis a decade ago. In his thesis [Nousiainen, 2002], he strongly advocated the use of statistical models for irregular particles; based on the results of Paper VI, I would say that statistical models are not necessarily able to model the realistic variation in scattering between the particles — a price to be paid for statistical averaging. It is true, however, that in practical applications these elaborate modeling approaches are far too time-consuming and, therefore, it is easy to agree with Nousiainen [2002] in that the need of simplifications in scattering problems is, indeed, continuous. Today, simplified models, publicly available light-scattering methods, and complete scattering databases facilitate the consideration of nonspherical particles. However, I would like to emphasize the need of appropriate validation of simplified approaches through comparisons to measurements — preferably at multiple wavelengths — or to representative computations. The dependence between the physical properties of a particle and its light scattering is so complex that it is recommended to consider validation aspects even though the same methodology had been successfully utilized in other contexts. After all, if the chosen modeling approach is not representative of its target, what value do the results have?

As discussed in Chapter 5, the modeling approaches developed in the thesis have already worked as an inspiration for further studies at multiple disciplines, including astronomy and biology in addition to atmospheric sciences. Moreover, the models in Papers II, III and IV have already

been applied to radiative impact estimations that consider the infrared radiation of volcanic dust [Kylling et al., 2013], the shortwave radiative flux of mineral dust [Haapanala et al., 2012], and the shortwave radiative impact of an ice cloud with special attention to the small, irregular crystals [Mauno et al., 2011], all considering particles more morphologically faithful to their targets than in previous studies. The shape distribution of spheroids that generally modeled best scattering by mineral dust derived in Paper III has even been notified for climate considerations by Räisänen et al. [2012] in the first-ever climate simulation accounting for nonspherical dust particles.

# References


Anderson, G., Clough, S., Kneizys, F., Chetwynd, J., and Shettle, E. (1986). AFGL atmospheric constituent profiles (0–120 km), Tech. Rep. AFGL-TR 86–0110, Air Force Geophys. Lab., Bedford, Mass.

Bailey, M. P. and Hallett, J. (2009). A comprehensive habit diagram for atmospheric ice crystals: confirmation from the laboratory, AIRS II, and other field studies. *J. Atmos. Sci.*, 66:2888–2899.

Baran, A. (2012). From the single-scattering properties of ice crystals to climate prediction: A way forward. *Atmos. Res.*, 112:45–69.

Berg, M. J. and Videen, G. (2011). Digital holographic imaging of aerosol particles in flight. *J. Quant. Spectrosc. Radiat. Transfer*, 112:1776–1783.

Bescond, A., Yon, J., Girasole, T., Jouen, C., Rozé, C., and Coppalle, A. (2013). Numerical investigation of the possibility to determine the primary particle size of fractal aggregates by measuring light depolarization. *J. Quant. Spectrosc. Radiat. Transfer*, 126:130–139.

Bi, L., Yang, P., Kattawar, G. W., and Kahn, R. (2010). Modeling optical properties of mineral aerosol particles by using nonsymmetric hexahedra. *Appl. Opt.*, 49:334–342.

Bohren, C. F. and Huffman, D. R. (1983). Absorption and scattering of light by small particles. John Wiley & Sons, Inc., New York.

Cattrall, C., Reagan, J., Thome, K., and Dubovik, O. (2005). Variability of aerosol and spectral lidar and backscatter and extinction ratios of key aerosol types derived from selected Aerosol Robotic Network locations. *J. Geophys. Res.*, 110, D10S11, doi:10.1029/2004JD005124.

Chýlek, P., Videen, G., Geldart, D. J. W., Dobbie, J. S., and Tso, H. C. W. (2000). Chapter 9: Effective medium approximations for heterogeneous particles. In Mishchenko, M. I., Hovenier, J. W., and Travis, L. D. (eds.): Light scattering by nonspherical particles, Academic Press, California.

Dabrowska, D. D., Muñoz, O., Moreno, F., Nousiainen, T., Zubko, E., and Marra, A. C. (2013). Experimental and simulated scattering matrices of small calcite particles at 647 nm. *J. Quant. Spectrosc. Radiat. Transfer*, 124:62–78.

Dabrowska, D. D., Muñoz, O., Moreno, F., Nousiainen, T., and Zubko, E. (2012). Effect of the orientation of the optic axis on simulated scattering matrix elements of small birefringent particles. *Opt. Lett.*, 37:3252–3254.

Debye, P. (1909). Der Lichtdruck auf Kugeln von Beliebigem Material. *Ann. Phys.*, 30:57–136.

Draine, B. T. and Flatau, P. J. (2009). User guide for the discrete dipole approximation code DDSCAT 7.0. Available at: http://arxiv.org/abs/0809.0337v5.

Draine, B. T. and Flatau, P. J. (1994). Discrete-dipole approximation for scattering calculations. *J. Opt. Soc. Am. A*, 11:1491–1499.

Draine, B. T. and Goodman, J. J. (1993). Beyond Clausius-Mossotti: Wave propagation on a polarizable point lattice and the discrete-dipole approximation. *Astrophys. J.*, 333:848–872.

Dubovik, O., Sinyuk, A., Lapyonok, T., Holben, B. N., Mishchenko, M., Yang, P., Eck, T. F., Volten, H., Muñoz, O., Veihelmann, B., van der Zande, W. J., Leon, J.-F., Sorokin, M., and Slutsker, I. (2006). Application of spheroid models to account for aerosol particle nonsphericity in remote sensing of desert dust. *J. Geophys. Res.*, 111, doi:10.1029/2005JD006619.

Edelsbrunner, H., Kirkpatrick, D. G., and Seidel, R. (1983). On the shape of a set of points in the plane. *IEEE T. Inform. Theory*, 29:551–559.

Falkovich, A., Ganor, E., Levin, Z., Formenti, P., and Rudich, Y. (2001). Chemical and mineralogical analysis of individual mineral dust particles. *J. Geophys. Res.*, 106:18029–18036.

Ginoux, P., Prospero, J. M., Gill, T. E., Hsu, N. C., and Zhao, M. (2012). Global-scale attribution of anthropogenic and natural dust sources and their emission rates based on MODIS Deep Blue aerosol products. *Rev. Geophys.*, 50:RG3005, doi:10.1029/2012RG000388.

Haapanala, P., Räisänen, P., Kahnert, M., and Nousiainen, T. (2012). Sensitivity of the shortwave radiative effect of dust on particle shape: Comparison of spheres and spheroids. *J. Geophys. Res.*, 117:D08201, doi:10.1029/2011JD017216.

Hakkarainen, H. (2011). Apple cultivar identification using automated shape analysis. Master's thesis, Dep. of Mathematics and Statistics, University of Helsinki.

Havemann, S. and Baran, A. J. (2001). Extension of *T*-matrix to scattering of electromagnetic plane waves by non-axisymmetric dielectric particles: application to hexagonal ice cylinders. *J. Quant. Spectrosc. Radiat. Transfer*, 70:139–158.

Heiken, G. and Wohletz, K. (1985). Volcanic ash. Univ. of Calif. Press, Berkeley.

Hill, S. C., Hill, A. C., and Barber, P. W. (1984). Light scattering by size/shape distributions of soil particles and spheroids. *Appl. Opt.*, 23:1025–1031.

Hoose, C. and Möhler, O. (2012). Heterogeneous ice nucleation on atmospheric aerosols: a review of results from laboratory experiments. *Atmos. Chem. Phys.*, 12:9817–9854.

Hu, R.-M. and Sokhi, R. S. (2009). Light scattering and absorption properties of dust particles retrieved from satellite measurements. *J. Quant. Spectrosc. Radiat. Transfer*, 110:1698–1705.

IPCC (the Intergovernmental Panel on Climate Change) (2007). Climate Change 2007 – The Physical Science Basis: Contribution of Working Group I to the Fourth Assessment Report on the IPCC. Cambridge University Press, Cambridge.

Jackson, J. D. (1999). Classical electrodynamics (3rd edition). John Wiley & Sons, Inc., New York.

Jacobs, K. M., Lu, J. Q., and Hu X.-H. (2009). Development of a diffraction imaging flow cytometer. *Opt. Lett.*, 34:2985–2987.

Jacobson, M. Z. (2001). Strong radiative heating due to the mixing state of black carbon in atmospheric aerosols. *Nature*, 409:695–697.

Kahnert, M., Nousiainen, T., and Lindqvist, H. (2013). Models for integrated and differential scattering optical properties of encapsulated light absorbing carbon aggregates. *Opt. Express*, 21:7974–7993.

Kahnert, M., Nousiainen, T., Lindqvist, H., and Ebert, M. (2012). Optical properties of light absorbing carbon aggregates mixed with sulfate: assessment of different model geometries for climate forcing calculations. *Opt. Express*, 20:10042–10058.

Kahnert, F. M. (2004). Reproducing the optical properties of fine desert dust aerosols using ensembles of simple model particles. *J. Quant. Spectrosc. Radiat. Transfer*, 85:231–249.

Kahnert, F. M. (2003). Numerical methods in electromagnetic scattering theory. *J. Quant. Spectrosc. Radiat. Transfer*, 79–80:775–824.

Kahnert, F. M., Stamnes, J. J., and Stamnes, K. (2002). Can simple particle shapes be used to model scalar optical properties of an ensemble of wavelength-sized particles with complex shapes? *J. Opt. Soc. Am. A*, 19:521–531.

Kahnert, F. M., Stamnes, J. J., and Stamnes, K. (2001). Application of the extended boundary condition method to homogeneous particles with point-group symmetries. *Appl. Opt.*, 40:3110–3123.

Kaye, P., Hirst, E., Greenaway, R., Ulanowski, Z., Hesse, E., DeMott, P., Saunders, C., and Connolly, P. (2008). Classifying atmospheric ice crystals by spatial light scattering. *Opt. Lett.*, 33:1545–1547.

Koehler, K. A., Kreidenweis, S. M., DeMott, P. J., Petters, M. D., Prenni, A. J., and Carrico, C. M. (2009). Hygroscopicity and cloud droplet activation of mineral dust aerosol. *Geophys. Res. Lett.*, 36:L08805, doi:10.1029/2009GL037348.

Krotkov, N. A., Flittner, D. E., Krueger, A. J., Kostinski, A., Riley, C., Rose, W., and Torres, O. (1999). Effect of particle non-sphericity on satellite monitoring of drifting volcanic ash clouds. *J. Quant. Spectrosc. Radiat. Transfer*, 63:613–630.

Kylling, A., Kahnert, M., Lindqvist, H., and Nousiainen, T. (2013). Volcanic ash infrared signature: Realistic ash particle shapes compared to spherical ash particles. *Atmos. Meas. Tech.* (submitted).

Laitinen, H. and Lumme, K. (1998). *T*-Matrix method for general star-shaped particles: First results. *J. Quant. Spectrosc. Radiat. Transfer*, 60:325–334.

Levasseur-Regourd, A.-C. and Hadamcik, E. (2003). Light scattering by irregular dust particles in the solar system: observations and interpretation by laboratory measurements. *J. Quant. Spectrosc. Radiat. Transfer*, 79–80:903–910.

Levasseur-Regourd, A.-C., Lindqvist, H., Brouet, Y., Hadamcik, E., Lasue, J., Määttänen, A., and Renard, J. B. (2013). Inner coma dust properties from polarization models. In: European Planetary Science Congress 2013, Sept 8–13, London, United Kingdom.

Liou, K. N. (1980). An introduction to atmospheric radiation. Int. Geophys. Ser., 26, Academic Press, New York, 392 p.

Liu, C., Panetta, R. L., Yang, P., Macke, A., and Baran, A. J. (2012). Modeling the scattering properties of mineral aerosols using concave fractal polyhedra. *Appl. Opt.*, 52:640–652.

Longtin, D. R., Shettle, E. P., Hummel, J. R., and Pryce, J. D. (1988). A wind dependent desert aerosol model: Radiative properties. AFGL-TR-88-0112, Air Force Geophysics Laboratory, Hanscom AFB, MA.

Lorenz, L. V. (1890). Lysbevaegelsen i og uden for en af plane Lysbolger belyst Kugle. *Det Kongelige Danske Videnskabernes Selskabs Skrifter*, 1:1–62.

Love, A. E. H. (1899). The scattering of electric waves by a dielectric sphere. *Proc. Lond. Math. Soc.*, 30:301–328.

Lumme, K. and Rahola, J. (1994). Light scattering by porous dust particles in the discrete-dipole approximation. *Astrophys. J.*, 425:653–667.

Macke, A., Francis, P. N., McFarquhar, G. M., and Kinne, S. (1998). The role of ice particle shapes and size distributions in the single scattering properties of cirrus clouds. *J. Atmos. Sci.*, 55:2874–2883.

Macke, A., Mishchenko, M. I., and Cairns, B. (1996). The influence of inclusions on light scattering by large ice particles. *J. Geophys. Res.*, 101:23311–23316.

Mauno, P., McFarquhar, G. M., Räisänen, P., Kahnert, M., Timlin, M. S., and Nousiainen, T. (2011). The influence of observed cirrus microphysical properties on shortwave radiation: A case study over Oklahoma. *J. Geophys. Res.*, 116:D22208, doi:10.1029/2011JD016058.

Mayer, B. and Kylling, A. (2005). Technical note: The libRadtran software package for radiative transfer calculations – Description and examples of use. *Atmos. Chem. Phys.*, 5:1855–1877.

McFarquhar, G. M., Yang, P., Macke, A., and Baran, A. J. (2002). A new parameterization of single scattering solar radiative properties for tropical anvils using observed ice crystal size and shape distributions. *J. Atmos. Sci.*, 59:2458–2478.

Middleton, N.J., Betzer, P.R., and Bull, P.A. (2001). Long-range transport of 'giant' aeolian quartz grains: linkage with discrete sedimentary sources and implications for protective particle transfer. *Mar. Geol.*, 177:411–417.

Mie, G. (1908). Beiträge zur Optik trüber Medien, speziell kolloidaler Metallösungen. *Ann. Phys.*, 330:377–445.

Min, M., Dominik, C., Hovenier, J. W., De Koter, A., and Waters, L. B. F. M. (2006). The 10 $\mu$m amorphous silicate feature of fractal aggregates and compact particles with complex shapes. *Astron. Astrophys.*, 445:1005–1014.

Mishchenko, M. I. (1991). Light scattering by randomly oriented axially symmetric particles. *J. Opt. Soc. Am. A*, 8:871–882.

Mishchenko, M. I. and Travis, L. D. (1998). Capabilities and limitations of a current FORTRAN implementation of the *T*-matrix method for randomly oriented, rotationally symmetric scatterers. *J. Quant. Spectrosc. Radiat. Transfer*, 60:309–324.

Mishchenko, M. I. and Travis, L. D. (1994). *T*-matrix computations of light scattering by large spheroidal particles. *Opt. Commun.*, 109:16–21.

Mishchenko, M. I., Travis, L. D., and Lacis, A. A. (2002). Scattering, absorption, and emission of light by small particles. Cambridge University Press, Cambridge.

Mishra, S., Tripathi, S., Aggarwal, S., and Arola, A. (2012). Optical properties of accumulation mode, polluted mineral dust: effects of particle shape, hematite content and semi-external mixing with carbonaceous species. *Tellus B*, 64:18536.

Mugnai, A. and Wiscombe, W. J. (1980). Scattering of radiation by moderately nonspherical particles. *J. Atmos. Sci.*, 37:1291–1307.

Muinonen, K., Nousiainen, T., Fast, P., Lumme, K., and Peltoniemi, J. I. (1996), Light scattering by Gaussian random particles: ray optics approximation. *J. Quant. Spectrosc. Radiat. Transfer*, 55:577–601.

Muinonen, K., Nousiainen, T., Lindqvist, H., Muñoz, O., and Videen, G. (2009). Light scattering by Gaussian particles with internal inclusions and roughened surfaces using ray optics. *J. Quant. Spectrosc. Radiat. Transfer*, 110:1628–1639.

Muinonen, K., Tyynelä, J., Zubko, E., Lindqvist, H., Penttilä, A., and Videen, G. (2011). Polarization of light backscattered by small particles. *J. Quant. Spectrosc. Radiat. Transfer*, 112:2193–2212.

Muinonen, K., Zubko, E., Tyynelä, J., Shkuratov, Y. G., and Videen, G. (2007). Light scattering by Gaussian random particles with discrete-dipole approximation. *J. Quant. Spectrosc. Radiat. Transfer*, 106:360–377.

Muñoz, O., Moreno, F., Guirado, D., Dabrowska, D. D., Volten, H., and Hovenier, J. W. (2012). The Amsterdam-Granada light scattering database. *J. Quant. Spectrosc. Radiat. Transfer*, 113:565–574.

Muñoz, O., Volten, H., Hovenier, J. W., Veihelmann, B., van der Zande, W. J., Waters, L. B. F. M., and Rose, W. I. (2004). Scattering matrices of volcanic ash particles of Mount St. Helens, Redoubt, and Mount Spurr Volcanoes. *J. Geophys. Res.*, 109:D16201.

Muñoz, O., Volten, H., de Haan, J. F., Vassen, W., and Hovenier, J. W. (2001). Experimental determination of scattering matrices of randomly oriented fly ash and clay particles at 442 and 633 nm. *J. Geophys. Res.*, 106:22833–22844.

Niemeier, U., Timmreck, C., Graf, H.-F., Kinne, S., Rast, S., and Self, S. (2009). Initial fate of fine ash and sulfur from large volcanic eruptions. *Atmos. Chem. Phys.*, 9:9043–9057.

Nousiainen, T. (2009). Optical modeling of mineral dust particles: A review. *J. Quant. Spectrosc. Radiat. Transfer*, 110(14–16):1261–1279.

Nousiainen, T. (2002). Light scattering by nonspherical atmospheric particles. Finnish Meteorological Institute Contributions, 37, Helsinki.

Nousiainen, T., Kahnert, M., and Lindqvist, H. (2011a). Can particle shape information be retrieved from light-scattering observations using spheroidal model particles? *J. Quant. Spectrosc. Radiat. Transfer*, 112:2213–2225.

Nousiainen, T., Kahnert, M., and Veihelmann, B. (2006). Light scattering modeling of small feldspar aerosol particles using polyhedral prisms and spheroids. *J. Quant. Spectrosc. Radiat. Transfer*, 101:471–487.

Nousiainen, T. and Kandler, K. (2014). Light scattering by atmospheric mineral dust particles. Light Scattering Reviews, Springer (in press).

Nousiainen, T., Muñoz, O., Lindqvist, H., Mauno, P., and Videen, G. (2011b). Light scattering by large Saharan dust particles: Comparison of modeling and experimental data for two samples. *J. Quant. Spectrosc. Radiat. Transfer*, 112:420–433.

Nousiainen, T. and Vermeulen, K. (2003). Comparison of measured single-scattering matrix of feldspar particles with *T*-matrix simulations using spheroids. *J. Quant. Spectrosc. Radiat. Transfer*, 79–80:1031–1042.

Nousiainen, T., Zubko, E., Niemi, J. V., Kupiainen, K., Lehtinen, M., Muinonen, K., and Videen, G. (2009). Single-scattering modeling of thin, birefringent mineral-dust flakes using the discrete-dipole approximation. *J. Geophys. Res.*, 114:D07207, doi:10.1029/2008JD011564.

Peltoniemi, J. I., Lumme, K., Muinonen, K., and Irvine W. M. (1989). Scattering of light by stochastically rough particles. *Appl. Opt.*, 28:4088–4095.

Purcell, E. M. and Pennypacker, C. R. (1973). Scattering and absorption of light by nonspherical dielectric grains. *Astrophys. J.*, 186:705–714.

Räisänen, P., Haapanala, P., Chung, C. E., Kahnert, M., Makkonen, R., Tonttila, J., and Nousiainen, T. (2012). Impact of dust particle non-sphericity on climate simulations. *Q. J. R. Meteorol. Soc.*, doi: 10.1002/qj.2084.

Lord Rayleigh (Strutt, J. W.) (1899). On the transmission of light through an atmosphere containing small particles in suspension, and on the origin of the blue of the sky. *Philos. Mag.*, 47:375–384.

Riikonen, M. (2011). Halot: Jääkidepilvien valoilmiöt. Tähtitieteellinen yhdistys Ursa ry, Helsinki.

Riikonen, M., Cowley, L., Schroeder, M., Pekkola, M., Öhman, T., and Hinz, C. (2007). Lowitz arcs. *Weather*, 62:252–256.

Riley, C. M., Rose, W. I., and Bluth, G. J. S. (2003). Quantitative shape measurements of distal volcanic ash. *J. Geophys. Res.*, 108:doi: 10.1029/2001JB000818.

Rose, W. I., Bluth, G. J. S., Schneider, D. J., Ernst, G. G. J., Riley, C. M., Henderson, L. J. and McGimsey, R. J. (2001). Observations of volcanic clouds in their first few days of atmospheric residence: the 1992 eruptions of Crater Peak, Mount Spurr Volcano, Alaska. *J. Geol.*, 109:677–694.

Russell, P. B., Bergstrom, R. W., Shinozuka, Y., Clarke, A. D., DeCarlo, P. F., Jimenez, J. L., Livingston, J. M., Redemann, J., Dubovik, O., and Strawa, A. (2010). Absorption Angstrom exponent in AERONET and related data as an indicator of aerosol composition. *Atmos. Chem. Phys.*, 10:1155–1169.

Ryder, C. L., Highwood, E. J., Rosenberg, P. D., Trembath, J., Brooke, J. K., Bart, M., Dean, A., Crosier, J., Dorsey, J., Brindley, H., Banks, J., Marsham, J. H., McQuaid, J. B., Sodemann, H., and Washington, R. (2013). Optical properties of Saharan dust aerosol and contribution from the coarse mode as measured during the Fennec 2011 aircraft campaign. *Atmos. Chem. Phys.*, 13:303–325.

Schnaiter, M., Kaye, P. H., Hirst, E., Ulanowski, Z., and Wagner, R. (2011). Exploring the surface roughness of small ice crystals by measuring high resolution angular scattering patterns. *Atti della Accademia Peloritana dei Pericolanti: Classe di Scienze Fisiche, Matematiche e Naturali*, 89: doi: 10.1478/C1V89S1P084.

Stamnes, K., Tsay, S., Wiscombe, W., and Jayaweera, K. (1988). A numerically stable algorithm for discrete-ordinate-method radiative transfer in multiple scattering and emitting layered media. *Appl. Opt.*, 27:2502–2509.

Strokotov, D. I., Moskalensky, A. E., Nekrasov, V. M., and Maltsev, V. P. (2011). Polarized light-scattering profile – advanced characterization of nonspherical particles with scanning flow cytometry. *Cytometry*, 79A:570–579.

Sun, W., Loeb, N. G., Videen, G., and Fu, Q. (2004). Examination of surface roughness on light scattering by long ice columns by use of a two-dimensional finite-difference time-domain algorithm. *Appl. Opt.*, 43:1957–1964.

Tape, W. and Moilanen, J. (2006). Atmospheric halos and the search for angle X. AGU, Washington, D. C., doi:10.1029/SP058.

Tyynelä, J., Muinonen, K., Zubko, E., and Videen, G. (2008). Interrelating scattering characteristics to internal electric fields for Gaussian-random-sphere particles. *J. Quant. Spectrosc. Radiat. Transfer*, 109:2207–2218.

Tyynelä, J., Zubko, E., Videen, G., and Muinonen, K. (2007). Interrelating angular scattering characteristics to internal electric fields for wavelength-scale spherical particles. *J. Quant. Spectrosc. Radiat. Transfer*, 106:520–534.

Ulanowski, Z., Hesse, E., Kaye, P. H., and Baran, A. J. (2006). Light scattering by complex ice-analogue crystals. *J. Quant. Spectrosc. Radiat. Transfer*, 100:382–392.

Um, J. and McFarquhar, G. M. (2011). Dependence of the single-scattering properties of small ice crystals on idealized shape models. *Atmos. Chem. Phys.*, 11:3159–3171.

Um, J. (2009). The microphysical and radiative properties of tropical cirrus from the 2006 Tropical Warm Pool International Cloud Experiment (TWP-ICE). Academic dissertation, University of Urbana-Champaign.

van de Hulst, H. C. (1981). Light scattering by small particles (2nd edition). Dover.

Virtanen, J., Muinonen, K., Lindqvist, H., Granvik, M., and Näränen, J. (2013). Efficient algorithms for space debris observations: streak classification and orbital analysis. In: XXVI Geophysics Days, May 21–22, Helsinki, Finland.

Vogelman, A. M. and Ackerman, T. P. (1995). Relating cirrus cloud properties to observed fluxes: A critical assessment. *J. Atmos. Sci.*, 52:4285–4301.

Volten, H., Muñoz, O., de Haan, J. F., Vassen, W., Hovenier, J. W., Muinonen, K., and Nousiainen, T. (2001). Scattering matrices of mineral aerosol particles at 441.6 nm and 632.8 nm. *J. Geophys. Res.*, 106:17375–17401.

Waterman, P. C. (1965). Matrix formulation of electromagnetic scattering. *Proc. IEEE*, 53:805–812.

Webb, A. R. and K. D. Copsey. (2011). Statistical pattern recognition (3rd edition). Wiley.

Worms, J.-C., Renard, J.-B., Levasseur-Regourd, A. C., and Hadamcik, E. Light scattering by dust particles in microgravity: the PROGRA2 achievements and results. *Adv. Space Res.*, 23:1257–1266.

Yang, P., Baum, B. A., Heymsfield, A. J., Hub, Y. X., Huang, H.-L., Tsay, S.-C., and Ackerman, S. (2003). Single scattering properties of droxtals. *J. Quant. Spectrosc. Radiat. Transfer*, 79–80:1159–1169.

Yang, P., Bi, L., Baum, B. A., Liou, K.-N., Kattawar, G. W., Mishchenko, M. I., and Cole, B. (2013). Spectrally consistent scattering, absorption, and polarization properties of atmospheric ice crystals at wavelengths from 0.2 to 100 $\mu$m. *J. Atmos. Sci.*, 70:330–347.

Yurkin, M. A. and Hoekstra, A. G. (2011). The discrete-dipole-approximation code ADDA: capabilities and known limitations. *J. Quant. Spectrosc. Radiat. Transfer*, 112:2234–2247.

Yurkin, M. A. and Hoekstra, A. G. (2007). The discrete dipole approximation: An overview and recent developments. *J. Quant. Spectrosc. Radiat. Transfer*, 106:558–589.

Zubko, E., Muinonen, K., Muñoz, O., Nousiainen, T., Shkuratov, Y., Sun, W., and Videen, G. (2013). Light scattering by feldspar particles: Comparison of model agglomerate debris particles with laboratory samples. *J. Quant. Spectrosc. Radiat. Transfer*, (in press).

Zubko, E., Petrov, D., Grynko, Y., Shkuratov, Y., Okamoto, H., Muinonen, K., Nousiainen, T., Kimura, H., Yamamoto, T., and Videen, G. (2010). Validity criteria of the discrete dipole approximation. *Appl. Opt.*, 49:1267–1279.